Some Physics Considerations for AHF Beam Profile Observation

W. C. Sellyey

1-23-02

Introduction

This document will describe materials and devices that are being considered for observing and measuring beam profiles in AHF. This discussion deals primarily with the physics design of profile observing devices as opposed to engineering considerations. No decisions or recommendations are made here as to what devices to use in any part of AHF. Traditionally harps are use in low average power density beam transports so mostly harps will be used in the beamlines from the Synchrotron to the firing sites. For this reason harps are discussed first. Some viewscreen may be used in a few places and therefore these will be discussed. Their main advantage is that they provide all possible projections of the beam profile in one measurement. There are many more issues to be examined for viewscreens than for harps, and so a relatively large part of this document deals with issues that concern viewscreens and other optical observation of beam profiles in both the beamlines and the Synchrotron.

Thus this document will describe some profile measurements using scintillators, lenses and optical image sensors. Therefore, after the harp discussion, a set of measurements featuring useful optical imaging techniques that were performed by the author about 10 years ago are discussed. This will be followed by a discussion of properties of some beam activated light producing materials and a discussion of possible types of cameras to use in an accelerator environment. A discussion of optics for high radiation environments will follow. The last sections will discuss specific imaging systems for both the beamlines and Synchrotron using concepts developed in the earlier sections. It is to be emphasized that this document is far from the last word on these subjects and can be changed and updated as needed.

Harps

Harps can be used anywhere in the beam transport to obtain projections of beam profiles in the direction perpendicular to the secondary emission (SEM) wires. For typical approximately elliptical beams it has been shown that three projections are adequate for characterizing the 2-D transverse distribution[31]. Some analysis needs to be done to determine how many projections will be needed in the regions after the beam is split into two or more fragments on its way to firing sites. Another potential problem with secondary emission devices is the great sensitivity of SEM to surface properties and coatings[32]. An attractive characteristic of harps is the potential for making time resolved profile measurements of individual microbunches in a pulse train. In this section first a harp based profile measurements for observing profile projections of beam pulses separated by 200 ns will be described. Then, by simplifying the electronics of the time resolved system, a slow profile measurement system will be arrived at.

As usual, all beam bunches in all (six) dimensions will be assumed Gaussia. A wire that intercepts the beam at the center of the distribution will collect a charge Q_p given by

$$Q_p = \frac{\varepsilon Q_o \Delta x}{s\sqrt{2\pi}}$$

where ε is the secondary emission coefficient, Q_o is the charge in the beam bunch, Δx is the wire width and s is the rms bunch spatial width. Many types of electronics can be used to process the charge from the wires. As an example a Gaussian filter can be used to stretch the bunch signal and to limit noise. If σ_t is the beam charge temporal width and σ_F is the filter temporal (Gaussian) width the width of the filtered output voltage waveform is

$$\left(1+\frac{\sigma_t^2}{\sigma_F^2}\right)^{1/2}\sigma_F$$

σ_t is about 10 ns and if σ_F=50 ns, than the contribution of the previous pulse is less than 0.1% when the pulse separation is 200 ns. Neglecting σ_t the peak voltage into a cable with impedance R will be

$$V_p=\frac{\varepsilon Q_o \Delta x R}{2\pi s \sigma_F}$$

Using the definition of s and assuming Gaussian noise distribution the error in s due to noise is

$$\Delta s=\frac{\Delta V}{2sV_t}\left[\sum x_i^4\right]^{1/2}$$

where ΔV is the rms voltage noise at the output of one amplifier amplifier, V_t is the sum of all the voltage signals from the stretchers which produce significant output and x_i are the wire coordinates relative to the beam centroid. The sum is limited to ±3s and can be approximated by an integral. The result is $32ms^4$ where m is the number of SEM wires per mm. The sum V_t can also be approximated by an integral and is $V_t=6.28msV_p$. Combining the above one obtains

$$\frac{\Delta s}{s}=\frac{5.05}{m^{1/2}}\frac{\sigma_F \Delta V}{\varepsilon Q_o \Delta x R}$$

There are hidden units in the constant 5.05 and these are $(mm)^{3/2}$. To get a specific error estimate the secondary emission yield was obtained from information on the design of the Fermilab Proton Driver[25] and it is ε=0.02. Let m=3/mm, Δx=0.1 mm, R=50 Ω, $Q_o=10^{11}$ particles = $1.6*10^{-8}$ C. ΔV is obtained from a stretcher amplifier designed and constructed for amplifying stripline signals[33]. This amplifier has a gain of 31.5 and a 3 db frequency of 30 MHz. The filter considered here has a 3 db frequency of 2.21 MHz, and thus will pass less noise than the 30 MHz amplifier. The noise referred to the input of the 30 MHz unit was 25 μV and this is used here as an overestimate of the noise. (The actual noise is probably less than one half of this value.) Inserting these numbers into the above formula gives s/Δs=432 and this is clearly an adequate result. If time resolved signals are not needed, the stretcher can be replaced with a low bandwidth charge sensitive amplifier that has a 50 Ω input and whose signal to noise will be considerably less than what is used here. Cable attenuation and dispersion are ignored here but should be evaluated in a final design.

Another type of analogue processing electronics is the one used for wire scanners and halo scraper in the LEDA Halo experiment[36]. The error due to noise in the electronics is reported as 30 fC and using this value results in an rms profile measurement error half of what is obtained with the stretcher. However the stretcher has a bandwidth 30 times

that of wire scanner electronics, and if this taken into account the electronic noise contributions may be nearly equal in the two types of electronics.

It is shown here that thermal conduction might spreads the heat deposited in a carbon wire fast enough so that it will not reach a destructive temperature. The equation describing heat flow in one dimension for constant heat capacity C and thermal conductivity K is

$$\frac{\partial^2 T}{\partial x^2} = \frac{C}{K}\frac{\partial T}{\partial t}$$

Where T and t are the temperature and time and x is the dimension parallel to the wire axis. Taking the origin at the center of a wire of length 2L solutions to this are

$$T = B\cos(\omega t)e^{-\frac{t}{\tau}}$$

The longest time constant is

$$\tau = \frac{2L^2}{\pi}\frac{C}{K}$$

For graphite the heat capacity is taken as C=1.43 J/(^{o}K cm^3), the thermal conductivity is assumed to be K=0.8 w/(^{o}K cm) and taking L=2.5cm, τ=7.1 s. This is short compared to the 25 s between beam pulses and thus the maximum temperature rise can be estimated as the sum of an instantaneous temperature rise that occurs when the beam pulse strikes the wire, plus an average temperature resulting from the entire wire radiating the average power deposited in the wire. (This is also a valid over estimate for any value of τ, but if τ is much greater than 25 s the average temperature is close to the maximum temperature.)

The maximum temperature change of a thin wire as a result of a high energy beam with a Gaussian distribution of rms width s is given by

$$\Delta T = \frac{dE}{dx}\frac{N}{2\pi C s^2}$$

dE/dx=2 MeV*cm^2/g*1.602*10^{-19} J/ev*2g/cm^3 = 6.4*10^{-13} J/cm for 50 GeV protons passing through graphite. Taking N=3*10^{13} and s=1 mm results in ΔT=213.7 ^{o}C. The average temperature of the wire is given by

$$T^4 = \frac{1}{\sqrt{8\pi}}\frac{dE}{dx}\frac{Nr}{2L\varepsilon\sigma s\Delta t} + T_a^4$$

The wire radius r =0.005 cm, the emissivity ε=0.8, T_a =300 K is the ambient temperature, Δt=25 s is the time between beam pulses and σ is the Stefan-Boltzmann constant. For these values T=327 K and the overestimated maximum temperature will be 327+214=541 K=268 ^{o}C.

Both C and K vary with temperature. The C used above is for about 600 K and this value is midway between its values at 300 K and 3500 K. The thermal conductivity depends heavily on how the fiber was prepared and is also temperature dependant. Thermal conductivity of Carbon varies over four orders of magnitude depending on the form of the substance. To avoid a possible overheating problem the maximum temperature of the carbon is also calculated assuming no thermal conduction. The maximum temperate (spike) at the center of the beam will be the same as before: 213.7 ^{o}C. The average temperature at the center of the distribution over Δt=25 s when the wire is at the beam center is

$$T^4 = \frac{dE}{dx}\frac{N_o r}{4\pi s^2 \varepsilon\sigma\Delta t} + T_a^4$$

This evaluates to T=523 K. Adding the spike temperature results in 465 ^oC.

As described above, 100 μm carbon wires can be used for 1 mm rms size beams. In some places, the beam will be about 1 cm rms. In that case 1 mm graphite rods could be used to get about the same signal amplitudes as in the 1 mm beam case. There is now the possibility that nuclear reactions will be important. To overestimate the temperature rise in this case, assume that the energy of all the protons removed from the beam is deposited in the rods as heat. The interaction length of protons in Carbon is given as 43.15 cm[26] and this results in an effective dE/dx=1.85*10^{-10} J/cm. An average temperature of 570 K =297 ^oC results for the case involving conduction and 671 K=398 ^oC for radiation only. The temperature spike will be 617 K and the overestimated maximum temperatures will be 914 ^oC and 1015 ^oC.

Despite the uncertainties in thermal conductivity and the temperature dependence of C an K, it is reasonably certain that there will be no overheating problems with Carbon wires. However it would be instructive and useful to do numeric calculations using accurate temperature varying C and K. This will be done by the author and described in a future paper.

Formulas for calculating the inductance and capacitance per unit length of parallel wires are well known[34]. For a pair of adjacent wires in a harp described above, the wire separation is 1/3 mm and the wire radius is 100 μm. For a wire length of 5 cm the capacitance is 0.742 pF and the inductance is 37.5 nF. The resistance of a 5 cm, 100 μm Graphite wire is about 100 Ω. Adding this to the 50 Ω cable impedance gives RC=0.11 ns, L/R=0.25 ns and $(LC)^{1/2}$=0.17 ns. All of these are small compared to the Gaussian filter rms time width (50 ns) and thus are expected to be unimportant.

Camera Measurements

The purpose of this discussion is to establish a simple but accurate way of characterizing resolution related quantities for cameras. It essentially consists of imaging a small spot on the camera faceplate. Some quick and simple ways of extracting things like full width at half maximum (FWHM) are also discussed. Finally a method for monitoring intensified camera resolution using single photoelectron events is discussed.

When beam transverse (charge) distributions are measured the results to first order, are almost always stated as an rms or FWHM value. Finer structures can be present and are sometimes observed. In all cases it is useful for the beam imaging system to have a δ-function response much smaller than the smallest detail being imaged on the camera faceplate. The δ-function response is here defined as the image that will be observed on an ideal display when a zero diameter photon beam strikes the camera faceplate. The FWHM, the rms of the δ-function response and average deviation are used in this discussion as the fundamental resolution unit.

It is assumed here that the δ-function distribution is a product of two distributions, one for a horizontal direction depending only on horizontal coordinates and one for the vertical direction depending only on the vertical coordinate. This is not the case when circular optical lenses are used in the system. It will be assumed in this part of the discussion that the lens resolution is unimportant. Lens effects will be discussed later.

The Fourier Transform of the δ-function response for a camera is called the Modulation Transfer Function (MTF). A good and frequently used method for determining the δ-function response is to measure the MTF. A set of measurements of this type is shown in figure 1 for a Xybion ISG-250 gated intensified camera. (The data was obtained from Xybion[19].) The MTF is well described by[17]:

$$MTF = Ae^{-(f/f_0)^n}$$

The quantities f_0 and n are characteristic of a camera. Taking the natural log of the above gives:

$$\ln(MTF) = \ln(A) - mf^n$$

Where $m=1/f_o^n$. A plot of the ISG-250 data is shown in figure 2 for n=1.2. This n value came about by trying various values until the line became straight. The slope m=-0.0081. This m and n were used to generate 2^{14} points that were FFT'd to produce the δ-function response shown in figure 3. It is clear that the δ-function is not Gaussian since the MTF is not Gaussian.

Camera manufacturers typically state camera resolution in TVL (TV lines) over the faceplate of an imaging tube. TVL/2 is approximately the spatial frequency at which the MTF has .03 of its value at 0 spatial frequency (technically it is actually the CTF[17]). If one knows m or n, the MTF curve and thus δ-function response might be deduced from this one value of MTF. However manufacturers usually do not measure or publish these numbers. Thus it is frequently not possible to get good FWHM or rms values for cameras without the user doing some measurements on the cameras.

Figure 4 shows the δ-function response for a VC2400 CCD camera. To generate it a HeNe laser shone on a 330 μm hole at a distance of 2 m from the camera. The image of the hole was focused on the camera faceplate through a 12.4 mm F1.4 lens. The Airy disk diameter was 2.4 μm and the diameter of the focused image was 2 μm. These can both be neglected because they are small compared to the pixel size of 11 μm X 13 μm. The lens focus was adjusted to get a minimum spot size, and the data of figure 4 was recorded. The rms width for the horizontal is 10.4 μm and for the vertical it is 8.6 μm.

Since δ-function response of a camera is not Gaussian, there is no simple way to relate rms and FWHM. A relatively elaborate way to obtain FWHM would be to fit the data with various bell shaped functions. To obtain simple graphical determination of FWHM a subset of the data was plotted and a polynomial of order one less than the number of points was made to pass through each point (figure 5). To damp out oscillations, one or two points on either end of the plot were adjusted in position and value. This gives 22.2 μm for the horizontal and 20 μm for the vertical.

Pulnix manufactures a CCD camera using the same chip as the VC2400. Their published[18] MTF curve is given in figure 6. A plot of some of these points as a function of spatial frequency with a 4'th order fit is shown in figure 7. This fit was used to generate the frequency response for use in an FFT. The results of this were used to generate the camera δ-function response shown in figure 8. Note the unphysical negative undershoot. This may be due to the lack of data points above 26/mm for the MTF. FWHM for this is 26 μm. It is clear that the method of imaging a 330 μm hole results in a FWHM comparable to what is determined by measured MTF's and thus the validity of the procedure is verified.

This same method was applied to measure the resolution of two gated intensified cameras. One was a Xybion ISG-250 and the other a Stanford Computer Optics 4 Quick 05 (4Q05). The same setup was used as for the VC2400 with the gated intensified camera replacing the CCD camera. Figure 9 shows a set of data taken in this way (labeled resolution) for the 4Q05. Figure 10 shows this data (vertically rescaled) after background subtraction and the calculated rms width is 33+/-2 μm. The error was calculated using

$$\Delta s = \frac{1}{2s}\frac{\Delta A}{A}\left[\sum_i x_i^4\right]^{\frac{1}{2}}$$

where s is the rms width, Δs is the error in s, A is the sum of all digitizer channel counts above background, ΔA is the error in these counts and x_i is the distance from the centroid a digitizer channel corresponds to. (Note that this is of the same form as was used with harps.) Here it was assumed that the error in the counts is the result of electronic noise and that this noise is the same on all channels. Thus ΔA was obtained by calculating the rms fluctuation of the background.

The gain of the intensified cameras looked at here is sufficiently high so that single photoelectrons can be observed. To do this an attenuated laser beam shone directly onto the camera faceplate so one could observe the beam profile. The gating time was then reduced until single photon events could be distinguished. An example data set of this kind is shown in figure 9 and with background correction in figure 10. The rms width for this is 43+/-13 μm, in satisfactory agreement with the resolution result above. The single photon width measurement is a lower limit of the camera resolution and is completely independent of optics used to generate an image on the camera faceplate. The only thing not taken into account in this measurement is the possible spread introduced when the electron crosses the space between the photocathode and the MCP and this is probably negligible. Thus the observation of single photons and the automatic determination of the averaged widths of many such events could be used to monitor performance of cameras installed in a beamline. Figure 11 shows similar results for the ISG-250.

Light Producing Materials and Processes

The table below summarizes characteristics of a number of scintillateors and light emitters that might be used for beam imaging in AHF.

	CsI((Tl)	YAG(Ce)	GSO(Ge)	BGO	LSO(Ce)	Al_2O_3(Cr)	OTR	Cerenkov
Photons/Mev*proton	56300	16700	9700	5400	29500	12000[7]	.002 [#]	1.5 [&]
Rad hardness(rad)	10^6	10^5	10^9	10^5	$10^{8\,(30)}$	$10^{13\,(5)}$	Not relevant	*
Peak emission Wavelength (nm)	560	550	430	480	415	693, 694[4]	flat	*
Decay constant (ns) fast/slow (ratio)	700/7000 (20/1)	88/300 (7/3)	56/600 (7/1)	60/300 (1/10)	11/36 (2/1)	5000000	0	0

[#]photons/(proton*100nm)

[&]Photons/(proton*mm*100 nm) for 500 nm light in fused silica.

*Depends on material used.

The data about the first five scintillators were obtained either directly from reference 1 or by combining information from reference 1 and 2. Errors in the photons/MeV are of the

order of 10%. The sixth column is $Al_2O_3(Cr)$ and it has been extensively studied in a number of forms. A coarse grained material was used and can be manufactured at SLAC by an electrolytic process[3]. Improved non-granular ceramic plates were developed in a cooperative effort between CERN and Morgan Matroc Ltd. Its light output was optimized for temperature stability, linearity and uniformity over the plate surface[5]. It was also tested for thermal shock resistance and found to be acceptable in this respect[6]. The error in photons/MeV for $Al_2O_3(Cr)$ is a factor of 3[7].

Optical Transition Radiation (OTR) was investigated and may be useful in the beamlines that take the protons to the experimental areas. OTR occurs whenever a charged particle transverses a medium boundary. When a proton enters a material surface where the normal to the surface makes an angle φ with the particle direction the backward OTR intensity *I* is given by[8]

$$\frac{dI}{d\omega, d\Omega} = \frac{e^2\beta^2}{4c\pi^3\varepsilon_0}\frac{\sin^2\theta}{(1-\beta^2\cos^2\vartheta)^2}\left|\frac{\varepsilon^{1/2}-1}{\varepsilon^{1/2}+1}\right|F(\theta,\phi)$$

Here θ and Ω are with respect to the direction of specular reflection, F is the Fresnel factor, e, c, ε_o, ω, and β have their usual EM and relativistic meanings and ε is the relative permittivity of the material. If the material is a metal with a shiny (perfectly reflecting) surface, ε is imaginary[9, 10] and F and the expression inside the absolute value sign are unity. The radiation is peaked in a cone that makes an angel of 1/γ with the direction of specular reflection. For 50 MeV protons, γ=53.3 and the opening half angle is $1/\gamma=1.08^o$. Approximating sinθ by θ and integrating to θ_m results in

$$\frac{dI}{d\omega} = \frac{e^2}{4c\pi^2\varepsilon_O\beta^2}(\ln(1+(\beta\gamma\theta_m)^2)-1+\frac{1}{(\beta\gamma\theta_m)^2})$$

Using ω=2πf, c=fλ, dω>Δω and the energy per photon E=hc/λ the number of photons produced per proton is

$$N = \frac{e^2}{2\pi\varepsilon_O\beta^2 ch}\left(\ln(1+(\beta\beta\theta_m)^2)-1+\frac{1}{(\beta\beta\theta_m)^2}\right)\frac{\Delta\lambda}{\lambda}$$

and h is Planks constant. With the fractional wavelength Δλ/λ=0.2 and $\theta_m=10/\gamma$ this evaluates to .0017 photons per proton. For $3*10^{13}$ protons the result is $5*10^{10}$ photons.

Cerenkov light is emitted in a cone around the path of a relativistic charged particle. The opening angle of the cone is $\cos^{-1}(1/n\beta)$ where n is the index of refraction. The number of photons emitted per unit length by a relativistic proton moving through a transparent medium is given by[11]

$$\frac{N}{L} = \frac{e^2}{2\varepsilon_O hc}\left(1-\frac{1}{n^2\beta^2}\right)\frac{\Delta\lambda}{\lambda^2}$$

Evaluating this for a 50 MeV proton in quartz at 500 nm and Δλ/λ=0.2 gives 1.5/mm*100nm. If the beam is perpendicular to the quartz plate exit surface, no light will

exit because Brewster's angle will be exceeded. A solution to this may be to put the quartz plate at 45^{O} to the beam direction, however this will cause the beam image to be spread over the thickness of the quartz plate. For 1 mm rms beams, this would require the quartz thickness to be reduced to around 0.1 mm. Furthermore, only a small fraction of the Cerenkov light will reach the camera. A solution that has been employed in the past, is to frost the light exit surface, so the light is hopefully scattered over all angles. The quartz will again have to be about .1 mm thick because of resolution considerations. With the frosting and thinning the light intensity at the camera will be about the same as with OTR.

Imaging Camera Considerations

Below is a list of different types of cameras that might be used to view and record beam images produced on the light producing materials described in the previous section. This list is by no means intended to be exhaustive. There are a large number of parameters that can be varied to define a beam profiling system. Among these are source light intensity and spectrum, lens system (which covers a subset of parameters), radiation tolerance or resistance, light sensor (another subset of parameters), cost, etc. Probably the dominant parameter is cost. As a rule, "off the shelf" items are less expensive than in house developed devices, and thus only "off the shelf" items are considered. The cameras selected are intended to sample available camera types whose characteristics overlap those likely to be useful in a beam imaging system. Array type detectors will be discussed later. Also only cameras whose suppliers provide adequate technical information are listed here. In some cases it will be possible to get an equally good camera at a lower price from another source.

Kodak DCS 420m[37]
Optical format: 13.8X9.2 mm
Readout: digital, programmable, not RS-170, readout time=0.175 s
Picture Elements: 1524 X 1012
Pixel Size: 9 X 9 μm
Limiting resolution: Not given; probably irrelevant
S/N ratio: 69 db
Pixel Well Depth: 45,000 electrons
Quantum Efficiency at 400 nm:1.2%; at 555 nm: 26%; at 700 nm: 17%.
Radiation tolerance: guess 10 kRad

Cohu model #2622 CCD, RS-170[12]
Price: $800
Optical format: ½" interline transfer
Picture Elements: 768(H) X 494(V)
Pixel Size: 8.4 μm (H) X 9.8 μm (V)
Limiting resolution: 580 horizontal TVL, 350 vertical TVL
Sensitivity: 0.65 lx full video
S/N ratio: 55 dB
Pixel Well Depth: 82,000 electrons

Quantum Efficiency at 400 nm: 13%; at 555 nm: 33%; at 700 nm: 43%.
Radiation tolerance: guess about 10 kRad

Princeton Instruments VersArray: 1300F cooled CCD system[13]
Price: $33,000
Readout: digital, programmable, not RS-170
Picture Elements: 1340 X 1300
Pixel Size: 20 X 20 μm
Resolution: Not given; probably irrelevant
Readout Noise: 4 electrons rms minimum
Pixel Well Depth: 200,000 electrons
Quantum Efficiency at 400 nm:13%; at 555 nm: 33%; at 700 nm: 43%.
Radiation tolerance: guess 10 kRad

Dage-MTI VE-1000 SIT, remote head, fiber optic faceplate, RS-170[14]
Price: $17000
Optical format: 1 ", 12.8 X 9.6 mm
Photo Cathode: Multialkali (Modified S-20)
CTF at 400 TVL: 43%
Limiting resolution: 700 TVL
Minimum usable picture: 10^{-4} lux
Max output at 10^{-2} lux
Quantum Efficiency at 400 nm: 15.5%; at 555 nm: 9.25%; at 700 nm: 2.04%.
Radiation tolerance: guess 10 kRad to 1 MRad

Dage-MTI 70R-2 Nuvicon, remote head, RS-170[14]
Price: $10,000.
Optical format: 1", 12.8 X 9.6 mm
Limiting resolution: 800 TVL
Dark current: 8 nA
Dark current illumination equivalent: 0.02 lux
Max linear: 1 lux, 500 nA
Max illumination: 10,000 lux
Radiation resistance: 100 MRad, experimentally verified in reactor environment 40% loss of output signal.

CIDTEC MegaRAD1, remote head, RS-170[15]
Price $2500.
Optical format: 2/3" , 8.8 mm X 6.6 mm
Picture Elements: 768(H) X 575(V)
Pixel Size: 11 μm (H) X 11 μm (V)
Limiting resolution: >500 TVL horizontal
Full Well capacity: 300,000 electrons
S/N ratio at full well: 47 db rms
Quantum Efficiency at 400 nm: 11.2%; at 555 nm: 21.4%; at 700 nm: 13.8%.

Radiation resistance: 1 MRad with no deterioration of performance, useful to 13 MRad, experimentally verified with Co^{60} γ source.

Xybion ISG750 gated intensified camera, RS-170, interline transfer[16]
Price:$21000.
Faceplate: Quartz
Optical format: 15.2 mm diagonal, 12.14 X 9.17 mm
Picture elements 756h X 484v pixels
Pixel well depth: 100000 electrons
Read noise: 178 electrons
Limiting resolution: 870 TVL
Quantum efficiency: 19% @ 400 nm; 36% @ 550 nm; 40% @ 700 nm
Optical gain: 40000
Phosphor: P-43 (green)
Quantum efficiency of CCD for green light: 60%
Radiation tolerance: guess about 10 kRad

Xybion IRO Gated Intensified Optics[16]
Price: $14000.
Faceplate: Quartz
Optical format: input=18mm, 13.6X10.2 mm , output= 2/3", 8.8 mm X 6.6 mm
Limiting resolution: 612 TVL
Quantum efficiency: 19% @ 400 nm; 36% @ 550 nm; 40% @ 700 nm
Optical gain: 40000
Phosphor: P-43 (green)
Radiation tolerance: guess about 10 to100 kRad

The table below summarizes camera characteristics of the above cameras in terms that are relevant for beam imaging.

1	2	3	4	5	6	7	8	9
Manufactu-rer , model, type	Radiation hardness (tolerance guess) MRad	Resolution TV lines H X V	Face-plate size H X V mm	Resolution FWHM HxV, μm	Size: H or V /FWHM	Signal/Noise as charge ratio: full well/noise [electrons/ photon] {single photon S/N}	Photon per pix or (FWHM rectangle) equivalent to noise @ wavelength nm	Photons per pix or (FWHM rectangle) for full well or signal @wavelength nm
Kodak DCS 420m	(.01)	None given	13.8X 9.2	18X18	767X 511	2250	$1.7*10^3$@400 77@555 118@700	$3.8*10^6$@400 $1.7*10^5$@555 $2.6*10^5$@700
Cohu 2622 CCD	(0.01)	580 X 350	6.4X 4.8	16.8X19.6	380, 245	562	$1.1*10^3$@400 $4.3*10^2$@555 $3.3*10^2$@700	$6.3*10^5$@400 $2.5*10^5$@555 $1.9*10^5$@700
P.I. 1300F Cooled CCD	(0.01)	None Given	26.8X 26	40X40	670, 650	50000 [1] {.25}	31@400 11@550 9@700	$1.6*10^6$@400 $6.1*10^5$@550 $4.7*10^5$@700
Dage VE100 SIT	(.01 to 1)	700	12.8X 9.6	46X34	278, 326	100 {.25}	(13)@400 (21)@550 (97)@700	$(1.3*10^3)$@400 $(2.1*10^3)$@550 $(9.7*10^3)$@700
Dage 70R-2	100	800	12.8X	40X30	320,	50	$(2.6*10^4)$@400	$(1.3*10^6)$@400

Nuvicon			9.6		329		$(1.4*10^4)$@550 $(1.6*10^5)$@700	$(8.3*10^5)$@550 $(8.1*10^5)$@700
Cidtec MRAD1 CID	10	500	8.8X 6.6	22X22	400, 300	227	$1.2*10^4$@400 $6.2*10^3$@550 $9.6*10^3$@700	$2.7*10^6$@400 $1.4*10^6$@550 $2.2*10^6$@700
Xybion ISG 750 ICCD	(0.01)	800	12.14X 9.17	39X29	311, 316	562 $[1.3*10^4]$ {21}	.07@400 .037@550 .033@700	39@400 21@550 19@700
Xybion IRO Intensifier	(0.01 to 0.1)	700	13.6X 10.2	56X42	242, 242			
Xybion IRO Intensifier + Cidtec MRAD1 CID	(0.01 to 0.1)		12.14X 9.17	62X52	219, 196	227 [952] {.13}	14.7@400 7.8@550 7.0@700	3333@400 1759@550 1573@700

The first column lists the various camera or camera subsystem described in the list of cameras above. The last entry (row) is a combination of an intensifier optically coupled to a CID camera. The data in the second column: Radiation hardness (tolerance guess) repeats what is stated in the lists. There is an important difference between radiation hardness and tolerance. Radiation hard indicates that a deliberate effort was made by the designer to make a device withstand high amounts of radiation, while radiation tolerance is the radiation amount a device happens to be able to withstand. Column 3 states the camera resolution in TV lines as stated by the manufacturer. Column 4, the faceplate size, is either obtained from the manufacturers direct specification or from the stated optical format. Column 5, Resolution FWHM, was taken as two pixel widths for cameras where the digital camera pixel size is expected to be dominant. The actual FWHM resolution is probably closer to one pixel in these cameras. For the ISG-250 and the 4Q05 it is approximately true that

$$\frac{F*W}{H}=1.255$$

where F is one half the limiting resolution stated by the manufacturer, W is the full FWHM and H is the dimension of the face plate (horizontal or vertical). This relation was used to estimate the FWHM of all other cameras in column 5. Column 6 is the horizontal and vertical dimension of the camera faceplate in units of FWHM. It is a measure of how much meaningful information can be observed by the camera in the space dimensions.

The last three columns deal with light intensity information, the conversion of photon into signal represented by electrons in the light detector element and various sources of noise. One source of noise is the statistical fluctuation of signal electrons produced by photons. For photoelectrons, the rms value of this noise is usually estimated as the square root of the number of accumulated electrons. Electrons are also produced by non-optical processes and are referred to as dark current. The noise produced by these electrons is also calculated as the square root of the number of electrons. A third important source of noise is the noise introduced by the electronics that transfers the signal plus integrated dark current from the light sensitive element to the processing electronics. This is the read noise.

Column 7 deals with signal to noise ratios (S/N) and related quantities. Unless otherwise indicated it is assumed that the light sensitive element is in a camera operating

in conformity with RS170 standards in an interline transfer mode. This means that the light sensitive element is exposed to photons in 1/30 s time intervals. Signal characteristics of cameras with other signal formats can be calculated from these results by scaling. For all cameras that use CCD's or CID's (digital cameras) as the final output detection element, the signal is taken as the maximum charge that can be stored in one pixel. This is called the full well capacity. When the full well capacity number is not available it is calculated using 1000 electrons/μm^2. Camera manufacturers usually give a noise specification in db without specifying the contributions from the various noise types. However for most situations encountered here, the read noise will dominate. To estimate the noise in electrons for a digital camera, the full well capacity is multiplied by the signal to noise ratio supplied by the manufacturer. Statistical noise will be ignored, although it may dominate in situations where the well is nearly full. For cameras that are not digital, signal to noise is calculated over a rectangle defined by the horizontal and vertical FWHM's (FWHM rectangle). Square brackets [] in column 7 contain the number of electrons resulting at the camera output for a photon that produced a photoelectron. Note that this excludes from consideration photons that entered the detector but did not generate a photoelectron.

When relevant, brackets {} contain the S/N for one electron events. The reason for calculating this number is that when it is grater than one, single photoelectron events can be observed. Unless indicated otherwise the noise was calculated using an area 4 times FWHM rectangle.

In columns 8 and 9 when the final photosensitive device is a digital device the entries are for one pixel. For other detectors the entries are for a rectangular area defined by FWHM rectangle. The numbers in these columns were calculated assuming a large number of photons evenly distributed over the camera faceplate divided by the number of pixels or FWHM rectangles contained in the faceplate.

Below is a detailed account of how the numbers in the last 3 columns were obtained for each camera:

Kodak DCS 420m: This camera contains a Kodak KAF-1600 imaging chip and specs for the camera are mostly obtained from the specs for this chip. The well depth is given as 45,000. All noise except statistical is given as 20 electrons and thus S/N=2250. Column 8 is obtained by dividing the noise by the quantum efficiency and column 9 results from dividing the well depth by the quantum efficiency.

Cohu 2622 CCD: The manufacturer specifies S/N=55 dB. As an electron ratio this is 562 and this is the entry in column 7. No quantum efficiency (QE) is available for this camera, so to get an estimate for column 8 and 9 entries it was assumed that the QE is the same as for 1300F described below. The column 9 entries were obtained by dividing the full well capacity by the QE. Column 8 is obtained by dividing column 9 entries by S/N.

P.I. 1300F cooled CCD: The dark current for this device at –50 C is 0.5e^-/s and is unimportant for a 1/30 s integration time. The read noise is 4 e's and this along with the full well capacity of 200,000 e's is used for calculating S/N (note that the statistical noise will equal the read noise at 16 signal electrons in the well). At the low photon energy available in the visible spectrum, a photon will produce at most one photoelectron in one pixel and thus [1]. Since the noise is 4e's, {0.25}. QE and full well capacity is used to calculate entries in column 9 and this is divided by s/n to get column 8.

Dage-MTI VE100 SIT: A minimum picture signal can be obtained at 10^{-4} lx and this signal is taken as the rms noise. The spectral response curve for this camera is close to that of the human eye, so this value is used as the true response in lx. At a wavelength of 550 nm 1w/m^2= 673 lx. In 1/30 s this will require 21.4 photons in a FWHM rectangle to generate the equivalent of the camera noise and this is the entry in column 8 at 550 nm (a 550nm photon has an energy of $3.614*10^{-19}$ J). QE's were calculated from the quantitative spectral response curve supplied by the camera tube manufacture and these are used to get the other two entries in column 8. A gain curve shows that the tube is linear to 10^{-2} lx and thus S/N = 100. This is used to get the entries column 9. The quantum efficiency of the intensifier tube is 0.0925 at 550 nm and therefore a single photoelectron will generate .5 times as much signal charge as the noise level (21.4X.0925=2). Assuming that this signal is spread over 4 FWHM rectangles, S/N for one photoelectron is 0.25. This is the entry in column 7 for the SIT camera {0.25}.
Dage-MTI 70R-2 Nuvicon The outstanding characteristic of this device is its 100 MRad hardness. The tube manufacturer specifies a dark current of 8 nA which, using a gain curve, corresponds to 0.02 lx illumination with a 2856K light source. About 80 % of the tube response to a 2856K source is in the infrared, and thus .1 lx of visible light would be needed to generate 8 nA of dark current. 0.1 lx is $4.13*10^{14}$ photons/m^2 at 550 nm and results in $1.64*10^4$ per FWHM rectangle in 1/30 s. This is the entry in column 8 at 550 nm. A relative spectral gain curve gives the other entries in this column. The gain curve also shows that the camera response is linear to 1 lx (2856 source) and thus S/N=50. Multiplying column 8 by 50 gives column 9.
Cidetec MRAD1 CID: The most important characteristic of this camera is its 10 MRad hardness. S/N is 47 dB, full well depth is 300,000 e's, and QE's are obtained from the absolute spectral gain curve. These result in the numbers in the last three columns.
Xibion ISG-750 Gated Intensified CCD Camera: The read noise of the CCD is 178 e's, and the well depth is 100,000e's. Therefore S/N=562. The optical gain for a 2856C source is 40000 and a factor of about 5 is needed to convert this to optical gain for visible light. The manufacturer has supplied a QE curve for the intensifier that gives .36 for 550 nm. The CCD has a .6 QE for the green light output of the intensifier. The number of electrons collected by the CCD for a photoeletron event is $1.44*10^4$ (=40000*.2*.6/.36). The 311X316 FWHM rectangles of the intensifier are mapped into the 756X464 pixels of the CCD an fiber optic coupler that results in a resolution rectangle on the CCD of 2.4 pixels by 1.5 pixels. The noise for a single photoelectron event is taken as that in 4 FWHM rectangles and this is 3.8*178=675 e's. The S/N for the photoelectron event is thus 21. QE and S/N are used to generate the numbers in columns 8 and 9 in the usual way.
Xybion IRO Gated Intensified Optics: The intensifier in this device is the same as the ISG-750 and the output is imaged onto any camera of the users choice by means of an optical system.
Xybion IRO Gated Intensified Optics + Cidetec MRAD1 CID: A possible combination would be to combine the IRO with the Rad hard MRAD1 to produce a somewhat radiation tolerant intensified camera. To estimate the resolution, the IRO and Mrad1 resolutions are added in quadrature. S/N is determined by the MRAD1. For the electrons per photoelectric event the QE=.6 of the CCD in the ISG-750 is replaced by the QE=.214 of the MRAD1 for 550 nm photons. A factor of .2 is needed to account for losses in the

optical coupling. The result is that 952 electrons are deposited in the CID for a photoelectron event. The FWHM rectangle of the intensifier maps into 4.1X3.4 pixels on the CID and four of these are used to estimate the noise as 7400 electrons. This results in a S/N=0.13

Optics for High Radiation Environments

There are three characteristics of optically transmitting materials that are affected by ionizing radiation and are of interest here. These are transient light attenuation, long term (permanent) light attenuation and fluorescence. There are two optical materials that have been demonstrated to have good properties in this regard. These are single crystal sapphire and fused silica. Small (25 mm) sapphire lenses are available but it is difficult to make larger lenses. The fluorescence of sapphire is about 1500 photons per MeV of deposited energy as compared to 10 photons per MeV for fused silica[20]. Thus sapphire has a potential for generating relatively high background signals. Therefore only fused silica will be discussed here, but this does not mean that sapphire should never be used.

The transient attenuation of fused silica was measured[21] in a pulsed reactor environment. Typical pulses were around 20 ms and 7 MRad. A typical attenuation coefficient was $7*10^{-4}$/mm. Peak short term doses in an accelerator environment are usually lower than 7 MRad, and thus this will have little effect on lenses a few mm thick. The permanent attenuation coefficient for fused silica after a dose of $2*10^{9}$ Rad has been measured[22] as function of wavelength. The largest value in the visible spectrum is 0.4/cm. The expected radiation dose for electronics near the Frmilab Main Injector is 50 Mrad[24] over the machine lifetime and therefore the radiation dose near the main AHF ring is assumed to be about 10 MRad. The largest thickness of fused silica that light will need to pass through in the discussions below is 7 cm. Thus the increased attenuation over the machine lifetime will be at most 1.4%. It is important to note that there can be large variations in radiation resistance properties (orders of magnitude) in materials obtained from different sources and irradiated in different ways. Thus whatever lenses are finally decided upon should be exposed to radiation levels comparable to what they will see during their expected lifetime. It is nearly certain that the average radiation levels in the beam lines will be much lower than in the ring, and thus there will be no problems with fused silica optics. The radiation levels could be so low that normal glass achromats could be used.

Several assumptions are made to get an order of magnitude estimate of radiation doses for devices along the transport beamlines. One assumption is that there will be a continuous fractional loss of beam of 10^{-7}/m. This fraction is the value predicted for the APT Linac[25]. Another assumption is that a lost proton will diverge from the beam centerline such that it will leave the vacuum in about half the separation between two quadrupoles. This separation is taken as 10 m. Assuming the beam tube radius is 2.5 cm, the average proton divergence angle is $5*10^{-3}$ radians. If the tube wall thickness is 1/16 inches, the proton will travel 31.7 cm in iron. The nuclear scattering length in iron is given as[26] 10.5 cm. Therefore nearly all surviving protons will be scattered. Assuming hard sphere scattering, the average scattering angle will be 90^{O} and the protons will on average be moving radially. Consider a fused silica device, such as a viewport at 10 cm from the beam. For a proton bunch of $3*10^{13}$ there will be 477/cm^2 radially moving protons. The nuclear interaction length of fused silica is 44 cm and therefore, on average

$5.2*10^{-5}$ J/cm^3 will be removed from the assumed 50 GeV radial proton beam flux. Assuming all this energy is deposited in the fused silica, it will receive a 5.2 kRad dose per $3*10^{13}$ bunch. If a beam pulse is delivered every 25 s, 8 hours per day, it will take 2.5 years to reach a dose of $2*10^9$ Rad. The dose calculated here is probably an overestimate by an order of magnitude and most instrumentation will be at least a meter from the beamline. Thus a camera 1 m from the beam may receive a dose of 2 MRad in 2.5 years.

In lens systems aberrations frequently need to be corrected to achieve some desired resolution (δ-function response). Chromatic and spherical aberrations for systems consisting of quartz spherical lenses will be considered here. When all lenses are made of the same material, it is possible to make two lens units which are achromatic at one wavelength in the sense that df/dn=0 at some specific wavelength and thus the combined focal length of the pair varies as $(\Delta n)^2$ where Δn is the deviation of the index of refraction from the value it had at the achromatic situation. To accomplish this, lenses are combined in pairs such that[27]

$$d = \frac{1}{2}(f_{10} + f_{20})$$

where f_{10} and f_{20} are the two lens focal lengths at the wavelength where df/dn=0 and d is their separation. (This is exactly valid only in the thin lens approximation, meaning that all lens thicknesses are set to zero.) As usual the combined focal length is:

$$\frac{1}{f} = \frac{1}{f_1} + \frac{1}{f_2} - \frac{d}{f_1 f_2}$$

For a single lens

$$\frac{1}{f_s} = (n-1)\left(\frac{1}{r_b} - \frac{1}{r_a}\right)$$

where f_s is the lens focal length and r_a and r_b are the radius of curvature of the two lens surfaces. It is convenient to replace the 1/r terms in the brackets by 1/R. Let n_o be the index of refraction for which the chromaticity condition is evaluated and let $n=n_o+\Delta$ with R1 and R2 referring to the two lenses. Than

$$\frac{1}{f} = \frac{1}{2(n_O - 1)}\left[\frac{1}{R1} + \frac{1}{R2}\right]\left[(n_O - 1)^2 - \Delta^2\right]$$

and to lowest order in Δ

$$\frac{\Delta f}{f_o} = \frac{\Delta^2}{(n_O - 1)^2}$$

where Δf is the difference between the focal length f_o at n_o and the focal length at n. For a single lens made of the same material and having a foal length the same as the combined system at n_o

$$\frac{\Delta f}{f_o} = \frac{-\Delta}{(n_O - 1)}$$

Lenses are typically designed to have a specified focal length f_o at some specified wavelength. To determine how important the effect of chromatic aberration is in a particular system, it is useful to calculate the average distance of rays hitting the image

plane from the location where a ray hits at the design wavelength. Figure 12 shows a ray coming from the left and entering a (zero thickness) lens. At the wavelength for which the lens is designed the ray would pass through the image point a distance I from the lens. For a different wavelength it will cross the optic axis at I-ΔI and thus will arrive at the image plane a distance α below the ideal image point. It is exactly true that

$$\frac{\alpha}{\Delta I} = \frac{r}{I - \Delta I}$$

ΔI is usually small and can be neglected compared to I and thus

$$\alpha = \frac{r\Delta I}{I}$$

For a spherical lens system, r is the distance from the center of the lens. To obtain the average aberration in a transverse direction Y, one needs to average the component of α in the Y direction over the quadrant of a circle as defined in figure 13. The result is

$$\overline{\alpha} = .424R\frac{\Delta I}{I}$$

For any lens

$$\frac{1}{f} = \frac{1}{I} + \frac{1}{O}$$

where f, I and O are the focal length, image distance and object distance. Taking the derivative with respect to I and substituting results in

$$\overline{\alpha} = .424R\frac{I}{f_O}\frac{\Delta f}{f_O}$$

For some situations considered here, the magnification will be small, I will be close to f_o and I/f_o will be taken as unity. In order to get the total average chromatic aberration, this expression has to be averaged over the wavelength range that is being used in a particular application. For a cylindrical lens 0.424 is replaced by 0.5 and R is the lens half width.

Figure 14 shows a plot of an LSO scintillator spectrum[28] and extrapolation pints obtained by fitting two polynomials to the data. Figure 15 shows a plot of n-1.4 as a function of wavelength for the index of refraction n for fused silica. Polynomial fits to this and figure 14 were used to calculate the average value of n and the average deviation Δn for any system using LSO and fused silica in an imaging system. (The camera's chromatic response is assumed flat over the region of interest. This of course is only approximately correct.) The average n=1.466507 and Δn=.0021. Putting these into the above equations the chromatic aberration for a single 5 cm diameter fused silica lens is 48 μm and for a two lens achromatic system it is 0.2 μm. For a 7.5 cm diameter lens, these numbers are 72 μm and 0.3 μm.

Spherical aberration is a consequence of the spherical shape of a lens. For rays passing close to the optic axis and making small angels with the axis, it is valid to set sin of angles equal to the angle. The focal length of a lens is defined using this approximation for a ray coming in parallel to the optic axis. The point where this ray crosses the optic axis is the focal point. In general, this is not a valid procedure and one needs to trace the ray through the lens using the full expressions in terms of sin and cos. When this is done the rays do not pass through the optic axis at the focal point. This deviation is referred to as spherical aberration.

Consider the pair of planoconvex lenses shown in figure 16. This combination reduces spherical aberration as compared to a single lens with the same focal length[27]. The radius of curvature of one lens is

$$R = (n-1)f$$

where f is the focal length. Let a light ray enter the system making an angle θ_{1in} with the optic axis at a distance y from the optic axis (y is not shown in the figure). Than, in the approximation that the lenses are of zero thickness, the following equations are used to calculate the exit angel θ_{2out}

$$\tan\phi = \frac{y}{R}$$

$$\sin\theta_{1in} = n\sin\theta_{1q}$$

$$n\sin(\phi - \vartheta_{1q}) = \sin\theta_{1out}$$

$$\theta_{2in} = -\theta_{1out} + 2\varphi$$

$$n\sin\vartheta_{2q} = \sin\theta_{2in}$$

$$\vartheta_{3q} = \varphi - \theta_{2q}$$

$$\sin\theta_{2out} = n\sin\theta_{3q}$$

Additionally it is useful to define the rays exit angel from the first lens relative to the optic axis. It is

$$\theta_{1ol} = \theta_{1out} - \phi$$

A program was written based on these equations to calculate the average aberration for the two lens systems just described and four lens achromatic systems described in the next section. This traces a large number (typically 10^7) of rays from a point object on the optic axis to a distributed image spot at the ideal image plane (the plane where all rays would converge to a point if there were no aberrations). The place where the ray enters the first lens is chosen using a random number generator. The average transverse arrival location of the rays is calculated and reported as the spherical aberration. All aberrations for spherical lenses calculated below were obtained using this program.

Imaging in the beam transport lines.

The lens systems discussed below were designed using the simplistic equations discussed in the previous section and therefore are incomplete. They are intended to illustrate what may be possible and what limitations exist when optical systems are used in high radiation environments. Before any such design is used to assemble hardware it needs to be redone and completed using ray tracing software like Zemax.

Figure 17 shows a fused silica lens combination that could be used to image beams of various sizes in a high radiation environment. The lens pair separation D is chosen so that chromatic aberration varies as $(\Delta n)^2$ around the wavelength for which the lens focal lengths are F_1=250 mm and F_2=100 mm. In practice, the exact value will depend on the color of the light being observed and this will be determined experimentally. The system design assumes that the lenses are of zero thickness.

Two specific cases will be considered here. The first assumes a relatively large beam dimension of 10 mm rms and a relatively low charge per bunch of 10^{11} protons. For this O, the object distance, is 2750 mm and I, the image distance, is 50 mm and the system magnification M=0.05. For an imager chip 8.8 mm across, the field of view is 176 mm or 6.93 in. The scintillator is .3 mm thick LSO. The first lens pair consists of 2r=75 mm diameter, 500 mm focal length fused silica lenses like Melles Griot LQF346. The second pair consist of 50 mm diameter, 200 mm focal length lenses like Melles Griot LQP 023. 10^{11} protons will produce $N_o=1.3*10^{15}$ photons when passing through 0.3 mm of LSO. A Gaussian charge distribution with s=10 mm rms width in both transverse directions is assumed (it will probably not be Gaussian) and the relatively noisy rad hard CID camera is used. The pixel dimensions are $\Delta x=\Delta y=11\mu m$. The number of photons arriving at a pixel from the center of a Gaussian distribution is

$$N_{pix} = \frac{N_o}{2\pi s^2}\frac{r^2}{4O^2}\frac{\Delta x \Delta y}{M^2}$$

This evaluates to $4.65*10^6$ photons per pixel at the maximum intensity of the beam. The full well capacity of the camera is reached with $2.7*10^6$ blue photons. The average spherical aberration is 110 μm. This corresponds to 2.2 mm on the GSO scintillator. If the beam size is 10 mm and it is added to the resolution in quadrature, the result is 10.2 mm. The additional 0.2 mm can probably be corrected by deconvolution. A better resolution of 32 μm can be achieved by stopping down the first lens to 50 mm diameter. The average chromatic aberration will be 0.3 μm at the camera and this will be unimportant.

The second system uses the same lenses with essentially the same separation (separations will differ slightly because of variations in the lens focal lengths with the index of refraction). This system is intended for use in the relatively high bunch charge areas of the beam transport and thus .3 mm thick Alumina screens are used. The typical beam size is assumed to be 1 mm, the magnification is 0.173, O=718.6 mm, I=67.6 mm and the field of view for a 8.8 mm camera face plate is 51 mm or 2 in. If the first lens is stopped down to a 50 mm opening, the spherical aberration at the camera will be .05 mm. At the screen this will be 0.3 mm and this can probably be mostly removed by deconvolution. The expected light intensity from the screen under many operating conditions will be such that the first lens will be stopped down to a fraction of 50 mm, and this will result in much better resolution.

Allison[29] has taken qualitative spectra of Alumina in the form of smudges on photographic film. These show two strong lines close to 700 nm spread over 5 nm and a broad background distribution spanning approximately 650 nm to 780 nm. The index of refraction of fused silica changes by less than 0.005 over this range and thus the chromatic aberration for a 5 cm lens aperture is about 0.3 μm. Protons passing through 0.3 mm of Alumina screen will produce about 1440 photons each. For a relatively low charge per bunch of 10^{11} protons and an aperture of 5 cm at the first lens, this will result in $2.7*10^7$ photons per pixel for the CID camera used above. For red light, $2.2*10^6$ photons per pixel are needed to fill the pixel well. Thus the first lens aperture can be stopped down in many cases, especially when looking at bunch charges one and two orders of magnitude higher than considered here. If fused silica lenses are used, the whole

spectrum will be available to the camera for imaging. This may not be the case if glass achromats are used.

The same lens arrangement as used with the Alumina screen could also be use in some places with OTR light. To do this replace the Alumina screen by a mirror finish Molybdenum sheet, D, I, O and the aperture are kept the same and the opening half angle will be 2^o. If light is accepted from 400 to 800 nm, $1.45*10^{-3}$ photons per proton will be sent into the optical system. For $3*10^{13}$ protons and the same beam size as before, $2.8*10^7$ photons per pixel will arrive at the center of the beam image on the CID chip. This will be about 10 times what is needed to fill the pixel well. Thus beam pulses of about $3*10^{11}$ protons and 1mm rms size could be imaged. Chromatic aberration will be about 1.2 microns and spherical aberration will be the same as in the Alumina case above.

The OTR light is a fairly broad beam much of which will not be intercepted by the lens arrangement used above. Small angular and lateral displacement of the light source can potentially cause large variations in signal strength arriving at the image plain. Thus the light arriving at the image plane will be a function of the beam position, foil orientation and foil smoothness. This could be overcome by using a much larger lens aperture, but this would increase spherical aberration. Thus a different lens design is desirable if OTR will be used. An acceptable design may not be possible using only fused silica lenses and mirror finish surfaces.

The two rad hard optical systems described above can also be implemented using non rad hard CCD cameras and normal glass lenses in shielded areas. This is primarily because much larger diameter off the shelf normal optical achromatic lenses are available. The equation above for N_{pix} can be solved for O and is

$$O = \frac{1}{2}\frac{r}{Ms}\sqrt{\frac{N_p}{N_{pix}}\Delta x \Delta y}$$

2r=150 mm achromats are readily available. For the CCD camera in the table above, the number of photons needed to fill a pixel with red (Alumina) light is $N_{pix}=1.9*10^5$, the pixel sizes are $\Delta x=8.4$ μm, $\Delta y=9.8$ μm, the number of photons produced by a 10^{11} bunch in a .3 mm thick screen is $N_p=1.44*10^{14}$. With M=.176 and s=1 mm the results are O=21.6 m. I=.176O=3.809 m and f=3.23 m. The f# is defined as the focal length divided by the lens diameter and is 21.5. A lens with f=3 m and diameter of 150 mm is available from Melles Griot (01 LAO 399). For the same situation accept that s=10 mm and M=.0176 the result is O=21.6 m, I=.374 m and f=.367 m. No lens like this is obviously available, but probably could be put together out of other lenses. The f#=2.5.

For the above two arrangements it is likely one can purchase off the shelf complex lenses with the correct f# that attach directly to a camera C-mount and will accomplish what is needed. These lenses will probably have smaller lens diameters, and therefore shorter focal lengths. This will make the images smaller than described above and a limiting factor will be the FWHM resolution of the camera.

Figure 18 shows a conceptual design of a scintillating viewscreen based beam imaging system. The beam strikes a thin scintillating material that emits light in proportion to the charge that passes through it. The mirror is used to eliminate possible image smearing caused by the finite thickness of the scintillator. For OTR imaging, the scintillaor is removed, and light from the mirror is used. For beam sizes large compared

to the scintillator thickness, the scintillator can replace the mirror. In most cases all lenses will be outside the beam vacuum, and thus the light from the viescreen will pass through a vieport. For high radiation environments, four lens achromatic optics could be used to control aberrations. The optics will generate a reduced size image of the beam directly on a camera faceplate.

Usable lifetimes of the GSO and Alumina screens will depend on the peak beam intensity. It will be assumed that each screen is used for an average of one hour per day and that operation is restricted to five day a week. It takes $2*10^8$ Rad of Co^{60} γ's to cause a 14 % darkening of 1 cm thick LSO[30]. Thus for a .3 mm thick piece of LSO, $1.78*10^3$ 1 mm rms proton bunches containing 10^{11} particles will darken the LSO by 14 %. Assuming 25 sec per cycle, the screen will last 1.2 hours or one day of operation. If there are 24 successive bunches in each synchrotron cycle, the screen will last only 3 minutes. The darkening of the LSO can mostly be reversed by heating at 300 ^oC for 1 day[30]. Thus if a means of heating is provided, the LSO may be usable indefinitely. This needs to be tested with beam. In most cases the LSO can be replaced by Alumina. Assuming it is bombarded with $3*10^{13}$ particles per 1 mm rms bunches, it will last at least 46 days. Heating can probably largely undo this radiation damage, but this has not yet been demonstrated. For $24*10^{11}$ 1 cm rms bunches on an Alumina the screen will last 20 years.

Some effects of beam heating on imaging view screens.

Two types of imaging view screens will be considered here: Alumina as a scintilltor and Molybdenum as an OTR screen. (LSO would be used at relatively low bunch charges and therefore will probably not be affected by beam heating.) It is first shown that the average temperature of these screens is only a few degrees. The maximum temperature is determined only by the temperature rise during the short beam macro-pulse. dE/dx=2 MeV*cm^2/g for all calculation done for this discussion and the number of protons per bunch is $N_o=3*10^{13}$. dE/dx will be written as $D(dE_s/dx)$ where $dE_s/dx=3.2*10^{-13}$ J*cm^2/g and D is the density. Emissivity ε for Alumina is 0.4 and for Mo it is 0.37; densities D are 3.97 g/$cm^3$and 10.22 g/cm^3; heat capacities C are 3.16 j/(cm^3 ^oC) and 2.57 j/(cm^3 ^oC); Melting temperatures are 2010 ^oC and 2617 ^oC; conductivities K are K=0.3 W/cm^oK and 1.35 W/cm^oK; material thickness L are 0.3 mm and 0.1 mm. The beam bunch is assumed to be Gaussian with s=1 mm rms width in both transverse directions. The average power deposited per unit length is

$$H = \frac{dE_s}{dx}\frac{N_o D}{\Delta t}$$

where Δt=25 s the time between two charge buckets. For Alumina this evaluates to H=1.526 W/cm and for Mo to 3.9 W/cm.

Neglecting radiation the temperature distribution in a cylinder of radius b in a cylindrically symmetric system can be calculated using the differential equation:

$$\frac{1}{r}\frac{\partial}{\partial r}\left(r\frac{\partial T}{\partial r}\right) = \frac{C}{K}\frac{\partial T}{\partial t}$$

where r is the distance from the origin and the cylinder center, T is the temperature and t is time. Solutions to this are of the form:

$$J_o(\gamma r)e^{-\frac{t}{\tau}}$$

$$\gamma^2 = \frac{C}{K\tau}$$

where $J_o(\gamma r)$ is the Bessel function of order 0. Only solutions for which $\partial J_o(\gamma r)/\partial r=0$ at the boundary of the cylinder are permitted. For the lowest "frequency" solution $\gamma b=3.832$. Letting b=2.5 cm one obtains τ=4.4 s for Alumina and for Mo it is 0.81 s. Beam pulses will occur every 25 s and thus there will be sufficient time for the heat to distribute over the entire screen.

Consider an infinitely long solid cylinder of radius b with a hole in its center of radius a. Let the surface at r=a and at r=b be T_a and T_b. Assuming K is constant it is easy to show that:

$$T_a - T_b = \frac{H}{2\pi K}\ln\frac{r_b}{r_a}$$

Let r_a=1 mm, a typical rms radius of the beam and r_b=25 mm, a typical radius of a view screen. For these values T_a- T_b=2.6 ^oC and 1.5 ^oC for Alumina and Mo respectively. These are an estimate of the temperature variation over the screen 25 or more seconds after a Synchrotron beam macro-pulse. Therefore it is a good approximation to consider the whole screen to be at the same temperature when calculating the temperature needed to radiate the average power being deposited into the screen.

The average screen temperature can be calculated with the following formula

$$T_2^4 = \frac{dE_s}{dx}\frac{LDN_o}{2\varepsilon\sigma\pi r_b^2\Delta t} + T_1^4$$

$$\sigma = 5.67 * 10^{-12}\frac{W}{cm^2K^4}$$

where T_2 is the screen temperature and T_1=300^{o}K is the ambient temperature. For both Alumina and Mo this is 305 ^{o}K. The conclusion is that the average screen temperature is less than 8 ^{o}C above ambient.

The peak temperature change is

$$\Delta T = \frac{dE_s}{dx}\frac{N_o D}{2\pi C s^2}$$

For Alumina this is 192 ^{o}C and for Mo it is 603 ^{o}C. The peak temperature of Alumina is thus around 225 ^{o}C well below 400 ^{o}C, the temperature where the light output starts to deviate from linear. For both Alumina and Mo the peak temperatures are far below their melting points.

Nuclear interactions are significant for 50 GeV protons. A calculation of deposited energy for 50 GeV protons as a function of material thickness has been done[35] and is shown in figure 19. This was used here to estimate the contribution of nuclear reaction products to the energy deposited in Alumina and Mo. The nuclear interaction lengths of W, Alumina and Mo are $\lambda_{W,A,M}$= 9.73, 24.9 and 15.9 cm. The amount of W that is penetrated by the proton beam which will produce about the same number of reaction products as .3 mm of Alumina is .3mm*(λ_W/λ_A)=0.12 mm. From figure 19 the ratio of nuclear to atomic energy deposition is about 0.7 and this is an estimate of the relative number of secondary particles that have been produced through nuclear reactions

in 0.3 mm of Alumina. The average number of secondary particles which deposit energy in 0.3 mm of Alumina will be half of this, so the effective dE/dx in Alumina will be multiplied by 1.35. To properly take this into account, all the temperature changes calculated above for Alumina need to be multiplied by 1.35. This results in a maximum temperature of 295 ^{o}C, which is an acceptable temperature. For Mo the temperature will be 643 ^{o}C.

The heat capacities and thermal conductivities of the materials discussed above are, as usual, functions of temperature. The heat capacities increase with temperature by about 30 % over the temperature ranges encountered here. This increase will tend to decrease the maximum temperatures and this will be a desirable effect. When the beam pulses are started, it will take about four accelerator cycles or 100 s to go half way between the ambient temperature and the final average temperature of 305 ^{o}C for the Alumina screen. Thus 100 s is a better estimate of the time available for the heat to distribute over the screen. The thermal conductivity of Alumina changes by a factor of two in the temperature range that the center of the screen will operate at. This will double τ=4.4 s, the characteristic time for distributing the heat. But there is actually 100 s available and therefore the approximation used here to under estimate maximum temperatures is still valid. Similar statements apply to Molybdenum.

Bunch by bunch observation of Synchrotron transverse profiles.

This system will be an RGIPM device and thus will measure only projections of the beam along one axis. For an RGIPM system approximately uniform and parallel electric and magnetic fields will need to be established in the region of the measurement. Many authors have described this type of system and the details of producing the fields will not be discussed here. The electron detection system will be designed so that (hopefully) a 5% measurement can be made in the rms width of a single bunch for each bunch on every turn in the Synchrotron. Additionally, the only detector component in the vacuum will be an LSO scintillator and this will be made as thin as possible to reduce unwanted background signals. The beam transverse distribution will be reproduced on the surface of the LSO by scintillation cased by 5 keV electrons accelerated and guided to the LSO by the E and B fields. This distribution will be viewed by an imaging system outside the vacuum.

Most RGIPM systems presently in operation use microchannel plates (MCP) in the vacuum chamber as signal amplifier. A problem with this is that the MCP's are limited in total charge they can produce per unit area. In time this leads to uneven gain over the MCP surface because, on average, transverse beam charge distributions are not uniform. The LSO scintillator will be used here in an attempt to circumvent this problem.

The light attenuation of LSO caused by Co^{60} γ's has been measured[30] and is quoted as 7% /(cm*10^{8}Rad) at the LSO emission wavelength. Assuming an average beam size of 2 mm rms, and that 7000 electrons are produced per cm which are then accelerated through a 5 kV potential (see below) it will take about ten days of continuously operating for 8 hr/day to reduce the LSO light transmission by 14 %. It has also been established that heating the LSO to 300 ^{o}C for about one day will restore it to essentially its original light transmission characteristic[30]. Thus by providing a means of heating the LSO (during times when the Synchrotron is not operating) it may be possible to use the same scintillator indefinitely. If permanent darkening is expected to developed

after say 100 heating cycles it would probably not be difficult to design the RGIPM such that the LSO could be easily replaced perhaps once every one or two years. It has been demonstrated that fused silica radiation damage can largely be reversed by heat. Thus the quartz viewport and lenses of this system might also be kept free of radiation darkening by making provisions for heating.

Assume that Xenon at a partial pressure of 10^{-7} torr is introduced into the beam tube at the measurement location. For Xenon a proton produces 44 (primary) electrons per cm at one atmosphere pressure[23]. If each bunch contains $1.25*10^{12}$ protons and the pressure is 10^{-7} torr, 7000 electrons per centimeter will be produced by each bunch. The ionization electrons will be accelerated through 5 kV before striking the LSO scintillator. Each electron will on average produce M=150 photons and a total of 10^6 photons will be produced per bunch of protons per cm. These photons will be focused onto 16, 0.8 mm wide by 18mm long cathode strips of a Hamamatsu R5900 multianode photomultiplier. Cylindrical optics will be used to image the photons. Also the lenses will be made of fused silica to minimize optical radiation damage. A pair of plano-cylindrical lenses with focal length of 100 mm will be used to produce a magnification of 2 at the photomultiplier faceplate. The width of these lenses will be 26 mm (Melles Griot LQC 006). A second cylindrical lens, perpendicular to the one just described, will be placed half way between the LSO sintillator and the photomeltiplier. Its width will be 26 mm and the focal length will be about 56 mm. It will probably consist of two lenses. This arrangement will focus .635 % of the photons from 16 mm of the beam onto the photomultiplier faceplate. The photomultiplier detection efficiency is 16% at the 420 nm wavelength of the LSO scintillation. Thus the overall detector efficiency will be $\varepsilon=0.16*0.00635=10^{-3}$. It can be shown that the fractional error in the rms width Σ is

$$\frac{\Delta\Sigma}{\Sigma}=\frac{1.225}{N^{1/2}M^{1/2}}\left[\frac{1}{\varepsilon}+0.0705N\frac{\Delta x}{\Sigma}\right]^{1/2}$$

Δx=0.5 mm is the sample width at the beam location and N=12600 is the total number of electrons produced in the 1.6 cm length of beam being imaged by the optics. Using this and Σ=1 mm and the values of ε and M given above results in $\Delta\Sigma/\Sigma$=0.034. If Nitrogen is used as the gas, the number of ionization electrons will be reduced by a factor of 0.23. In that case N=2900 and $\Delta\Sigma/\Sigma$=0.062. Note that these results do not contain errors resulting from the finite delta function response of the RGIPM measurement process, background correction, etc.

Formulas discussed earlier can be used to calculate the effect of circular shape of the lens surfaces (spherical aberration). The average spherical aberration is 11 μm at the image plane. The average chromatic aberration is 88 μm. The 1 mm pitch of the photomultiplier cathodes dominates the resolution. With the times 2 magnification it imposes a 0.5 mm FWHM resolution limit. The 88 μm aberration does not present any limitations on the measurement and it can be corrected for. For a complete analysis of the optics to include all distortions and aberrations a ray trace program like Zemax should to be used.

The field of view with one R5600 will be restricted to 8 mm. For larger fields of view, more R5600's will be needed probably each with its own lens system. Thus for about a one inch field of view, three R5600's will be needed. Higher resolution can probably also be obtained by increasing the magnification but proportionately more

R5600's will be needed to maintain the same field of view. An interesting possibility is that the lens and detector positions could be moved so that the magnification changes during the acceleration cycle.

The output of the PMT anodes will go to stretcher amplifiers of the same type as is discussed for the harps. Although the processing electronics will be analog, the fluctuation in the signal will be dominated by the statistical nature of the number of electrons arriving at each cathode and therefore formulas developed above are valid for error calculations.

A discussion of an RGIPM is not complete unless one looks at what happens to the molecules that are overlapped by the beam. The rms velocity of a molecule in an ideal gas is given by

$$v_{rms} = \sqrt{\frac{3kT}{m}}$$

and the average velocity $v_a=.92v_{rms}$. Evaluating this for N_2 gas at room temperature and calculating how far a molecule will move in the time between bunches one obtains 9.4 μm. The peak particle density in one bunch with 2 mm rms width is $5*10^{12}/cm^2$, each proton will produce 10 electrons per cm at STP and thus $5*10^{13}/cm^3$ are produced. There are $2.69*10^{16}$ nitrogen molecules per cm^3 at STP and thus the fraction of ionized molecules at the center of the beam bunch is $1.8*10^{-4}$. It will take 56 bunches to ionize 1% of the molecules and in this time a molecule traveling at the average speed will move 0.74 mm. The ionized Nitrogen molecules will moved about 1.4 cm in 200 ns, effectively removing them from the beam/gas interaction region and removing about 1% of the gas at the beam core during the time that 56 bunches pass by. Molecules that move at the average speed will be mostly replaced by molecules from regions not effected by the beam (3.7 times rms widths away) but a significant fraction of gas molecules will have velocities less than a fraction of the average and some will come from depleted regions. Consequently these molecules will not completely replace their removed counterparts and a net reduction in gas density will develop in the beam/gas interaction region. However the numbers here indicate that these will be on the order of 1% and thus if only 2% to 5% measurements are needed, one does not need to be concerned with this. However a detailed calculation of the importance of this effect at some time may be instructive.

2D time resolved proton bunch observation in the beam transport lines with an intensified camera.

The statistical error in the measured rms fractional width $\Delta\Sigma/\Sigma$ of a lens imaged Gaussian shaped beam profile is

$$\frac{\Delta\Sigma}{\Sigma} = 1.334\frac{\Sigma}{N_d^{1/2}}$$

and N_d is the total number of detected photons. For a 5% measurement ($\Delta\Sigma/\Sigma=.05$) $N_d=600$. As discussed earlier, 10^{11} protons passing through 0.3 mm of LSO will produce $N_p=1.3*10^{15}$ photons. The distance the lens for a camera can be placed from the screen such that the camera detects N_d photons is

$$R = \frac{r}{2}\sqrt{\frac{\varepsilon_q N_p}{N_d}}$$

here r=2.5 cm is the lens radius and ε_d=0.15 is the product of the camera quantum efficiency and light transport efficiency. The result is R=7.1 km. Thus a single gated intensified camera running in the single photon detection mode could, in principle, look at beam almost anywhere in the transport lines and at the same time be located in a well shielded area. The longest photon emission lifetime for LSO is 33 ns and thus individual bunches could be observed with the gated camera.

Since LSO is relatively sensitive to radiation damage, in may be desirable to use OTR light to image beams. If mirror surfaces are used the opening angle is impractically large thus it may be useful to investigate rough but shiny metal surfaces in the hope that backward OTR light would be spread out uniformly over a hemisphere. The Xybion 750 discussed earlier has an average quantum efficiency of 30 % in the 400 t0 800 nm range. For 10^{11} protons $1.8*10^9$ photons are spread into one hemisphere in this wavelength range. Assuming such a surface can be generated, and if a 150 mm diameter achromat is used to focus the light on the camera and ε_d=0.15 one obtains R=27.3 m. With a magnification of .176 the camera will be at a total distance of 32 m from the beam in a safe, shielded are.

References

1) V. V. Avdeichikof et. el., "Light output and energy resolution of CsI, YAG, GSO, BGO and LSO scintillators for light ions", Nuclear Instruments and Methods in Physics Research A 349 (1994) 216-224
2) T. Ludziejewski et. el., "Investigation of some scintillation properties of YAG:Ce crystals", Nuclear Instruments and Methods in Physics Research A 398 (1997) 287-294
3) R. W. Allison et. el., U. S. Patent 3,580,822 "Method For Producing A Chromium Activated Aluminum Oxide Scintillator" July 7, 1969
4) H. W. Leverenz, "An Introduction To Luminescence of Solids", John Wiley & Sons, 1950, page 255
5) C. D. Johnson, "The Development and Use of Alumina Ceramic Fluorescent Screens" CERN PS 90-42 AR
6) C. D. Johnson, private communication, the actual data on shock resistance has been lost.
7) Deduced from measurements made by the author in 1991 at Boeing Aerospace. See appendix for details.
8) D. W. Rule, R. B. Fiorito, "The Use Of Transition Radiation As A Diagnostic For Intense Beams", NSWC 84-134, Naval Surface Weapons Center, Dahlgren, Virginia 22448, Silver Springs, Maryland 20910
9) D. W. Rule, Private Communication
10) M. A. Omar "Elementary Solid State Physics", Addison-Wesley Publishing Co., Page 166
11) R. G. Lerner, G. T. Trigg, editors, "Encyclopedia of Physics", Second Edition, VCH Publishing, INC., 1990, p 130
12) Cohu Electronics Division web page: http://www.cohu-cameras.com/
13) Roper Scientific web page: http://www.roperscientific.com/
14) Peggy Jones, Dage-MTI, Inc.private communication
15) Thermo CIDTEC web page: http://www.cidtec.com/

16) Xibion Electronics Systems web page: http://www.xybion.com/xesprod.htm
17) "RCA Electro-Optics Handbook", Electro Optics and Devices, Lancaster, Pa.
18) Pulnix America web site: http://www.pulnix.com/
19) J. H. Lewis, "Modulation Transfer Function Measurement for Solid-State Intensified Cameras", Article number 1155-03, Xybion Electronics Systems Corporation, 8380 Miralani Drive, San Diego, California 92126
20) T. Nishitina, E. Ishitsuka, T. Kakuta, H. Sagawa, K. Noda, Y. Oyama, T. Iida, T. Ssugei, H. Kawamura, S. Kasai, "Japanese contribution to ITER task of irradiation tests on diagnostics components" Fusion Engineering and Design 42 (1998) 443-448.
21) G. H. Miley, O. Barnouin, J. Nader, W. Williams, A. Procoli, "Influence of high-intensity radiation on the properties of optics for fusion diagnostics", Fusion Engineering and Design 18 (1991) 341-348.
22) A. Morono, E. R. Hodgson, "Radiation induced optical absorption and radioluminescence in electron irradiated SiO_2", journal of nuclear materials, 258-263 (1998) 1889-1892.
23) F. Sauli
24) W. Chou, C. Ankenbrand and E. Malamud for the Proton Driver Design Study Group, "The Proton Driver Design Study", Fermilab-TM-2136, December 2000.
25) James F. Jackson presentation to the Energy Research Advisory Board, "Accelerator Production of Tritium", October 25, 1989
26) D. E. Gordon, revised the Atomic and Nuclear Properties of Matter in the European Physical Journal, Review of Particle Physics, page 80, V 15, Number 1-4, 2000
27) J. A. Melles, editor, Melles Griot Inc., "Optics Guide 5" , 1990
28) C. L. Melcher and J. S. Schweitzer, "Cerium-doped Lutetium Oxyorthosilicate: A Fast, Efficient New Scintillator", IEEE TRANSACTIONS ON NUCLEAR SCIENCE, VOL. 39,NO 4, 1992
29) R. W. Allison, Jr., R. W. Brokoff, R. L. McLaughlin, R. M. Richtere, M. Tekawa, and J. R. Woodyard, " A RADIATION-RESISTANT CHROMIUM-ACTIVATED ALUMINUM OXIDE SCINTILLATOR", UCRL-19270, UC-37 Instruments, TID-4600 (54th Ed.), July 16, 1969
30) M. Kobayashi, M. Ishii, C. L. Melcher, "RADIATION-DAMAGE OF A CERIUM-DOPED LUTHENIUM OXYORTHOSILCATE SINGLE-CRYSTAL" Nuclear Instruments and Methods In Physics Research Section A, v .335(#3) pp. 509-512 Nov 1, 1993
31) J. s. Fraser, "BEAM ANALYSIS TOMOGRAPHY", IEEE Transactions on Nuclerar Science, Vol. NS-26, No. 1, February 1979
32) P. E. Best, "Secondary Electron Emission" in Encyclopedia Of Physics, VCH Publishers, Inc., 2nd edition, Edited by R. G. Lerner and G. L Trigg, 1991
33) W. C. Sellyey and R. W. Kruse, "Operational Amplifier Based Stretcher for Stripline Beam Position Monitors", 1991 IEEE Particle Accelerator Conference, San Francisco, California, pp. 1145-1147, May 1991.
34) E. M. Pugh, E. W. Pugh, Principles of Electricity and Magnetism, 2nd Eddition, Addison-Wesley Publishing Company, 1970
35) Private communication, Andy Jason, LANL

36) M. E. Gruchalla, J. O'Hara, D. Barr, T. Cote, L. Day, D. Gilpatrick, M. Stettler, "BEAM PROFILE WIRE-SCANNER/HALO-SCRAPER SENSOR ANALOG INTERFACE ELECTRONICS", 2000 PAC, Chicago Ill.
37) "KAF-1600L 1526(H)X1024(V) Full-Frame CCD Image Sensor Monochrme with Anti-Blooming Performance Specifications" Eastman Kodak Company, Microelectronics Division, Rochester, New York 14650, Revision 1, June 26, 1995.

Figure 1. ISG-250 Modulation Transfer Function

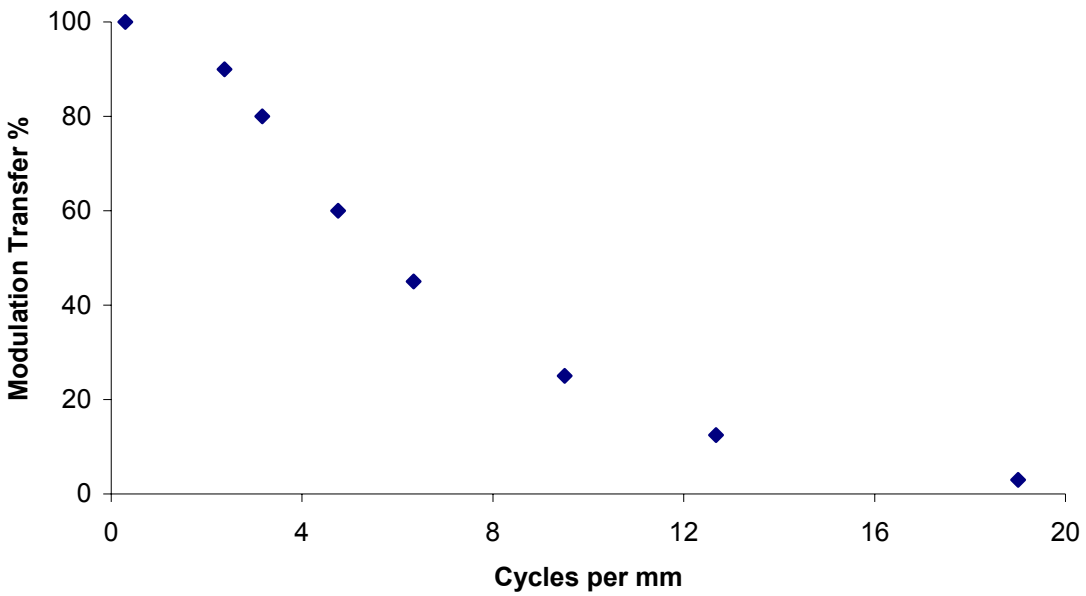

Figure 2. Determination of Slope and Exponent

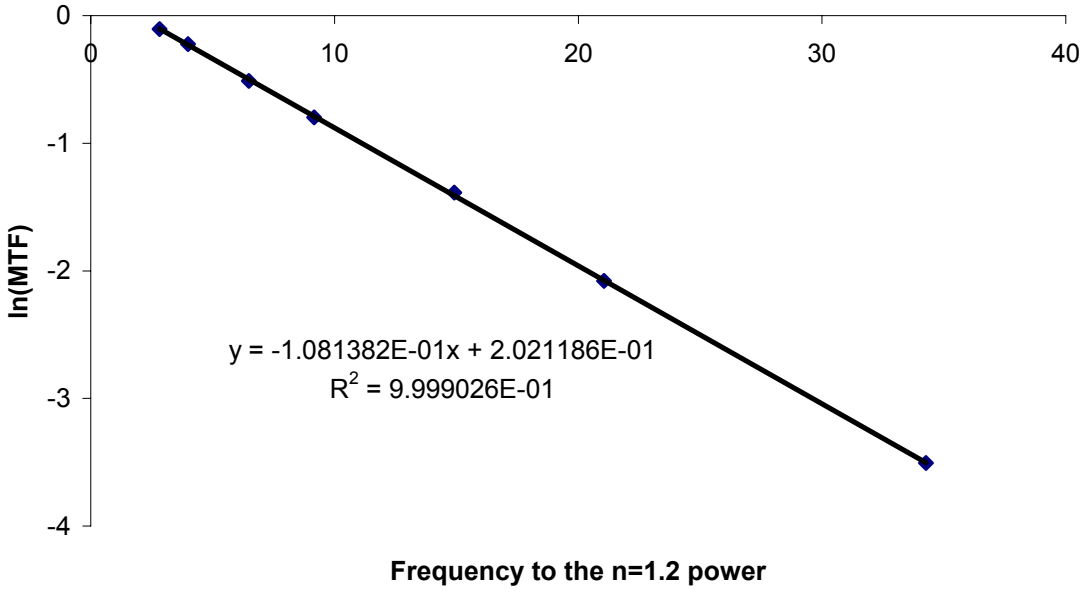

Figure 3. ISG-250 Delta Function Response

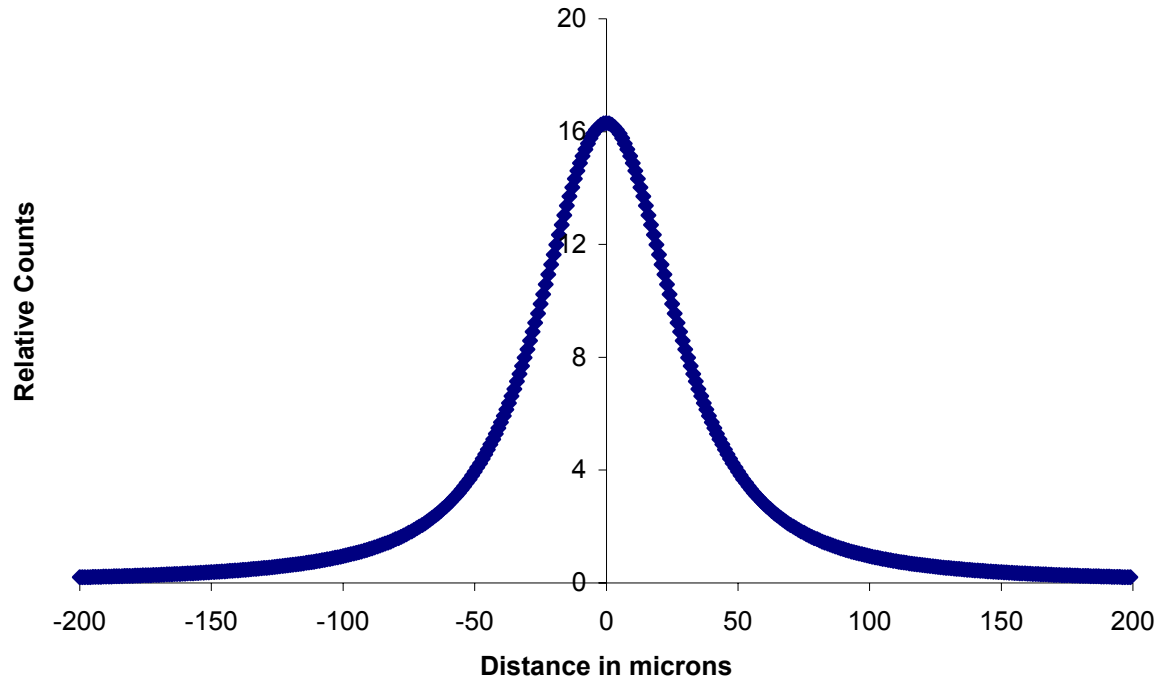

Figure 4. Delta function Response of VC2400 CCD camera

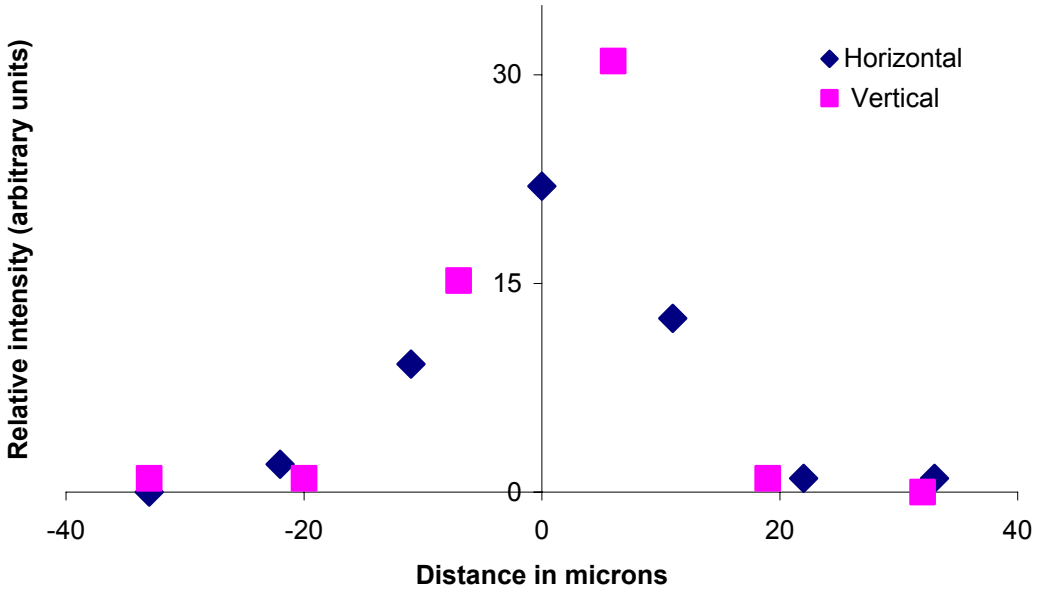

-

Figure 5 Graphical Determination of FWHM for VC2400 CCD

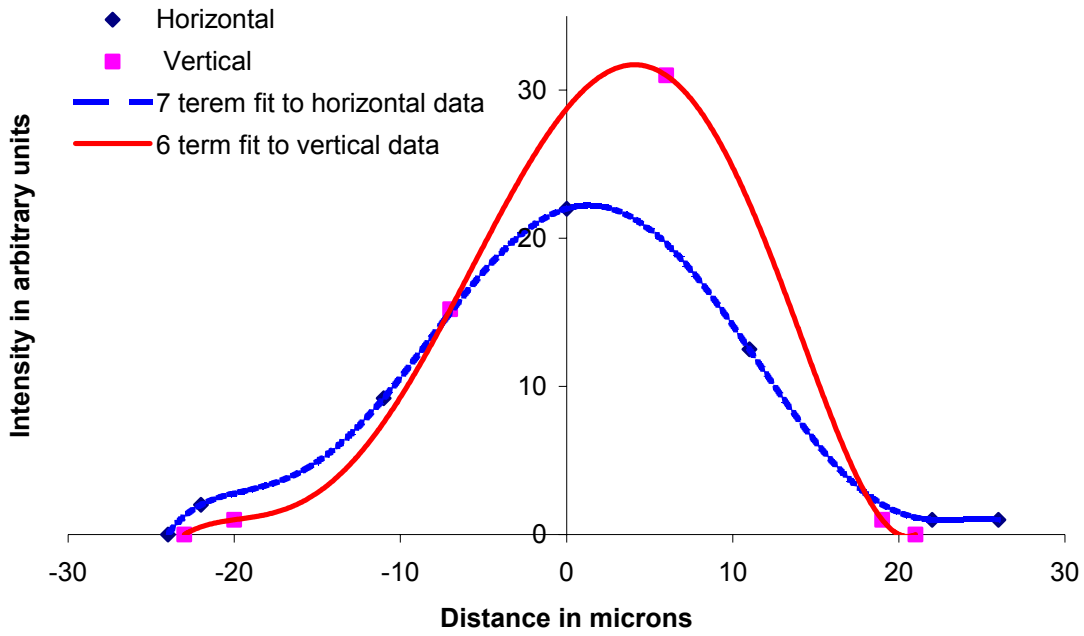

Figure 6 Modulation transfer function for TM475 CCD camera

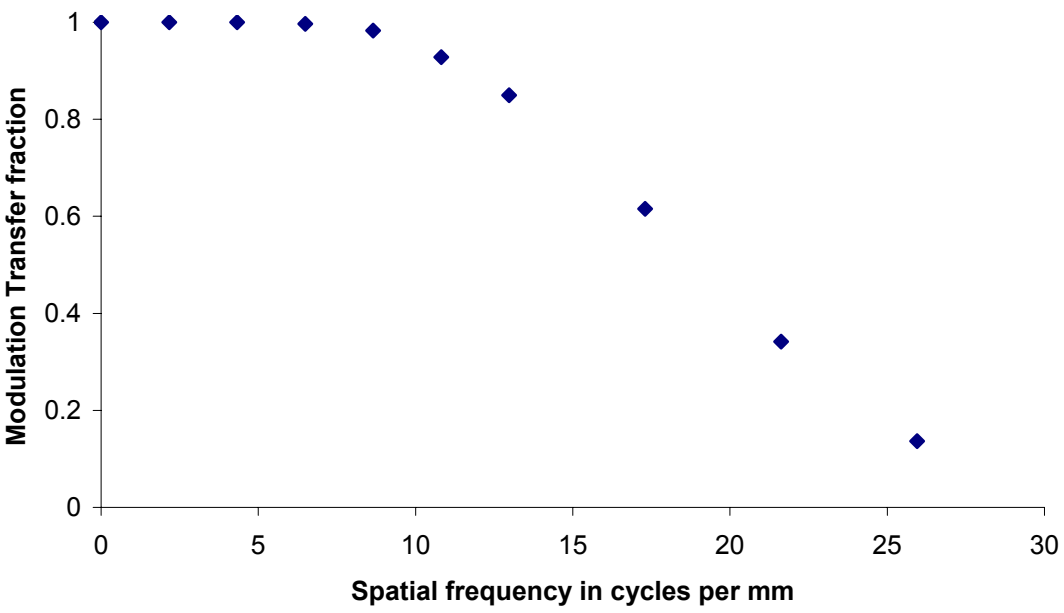

Figure 7. 4'th order fit to TM745 MTF data.

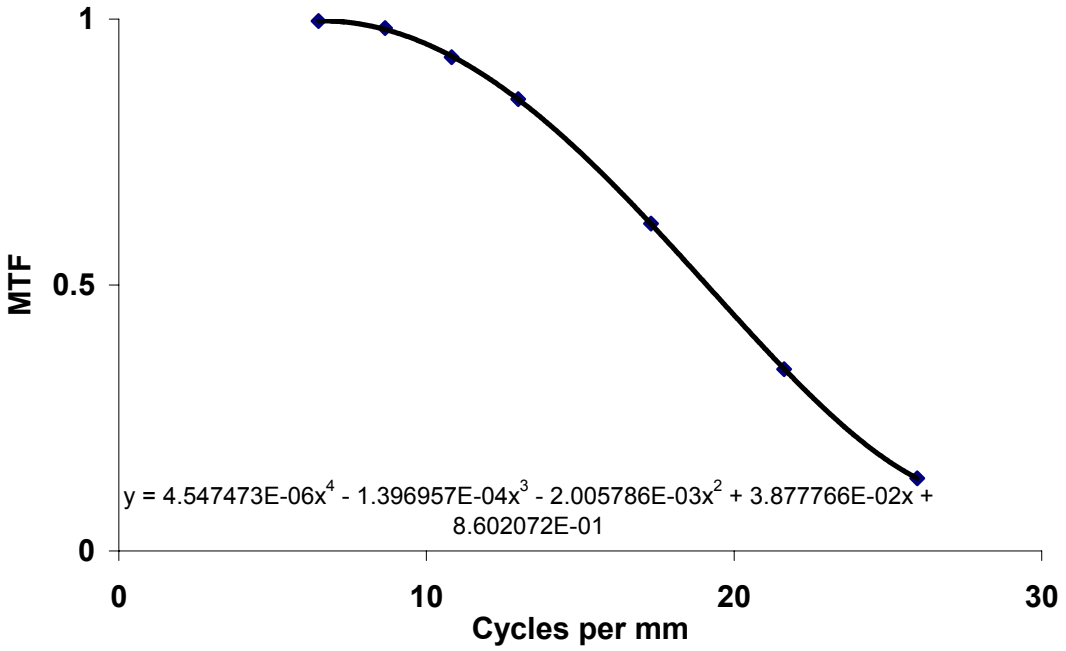

Figure 8. Delta Function Response of TM745

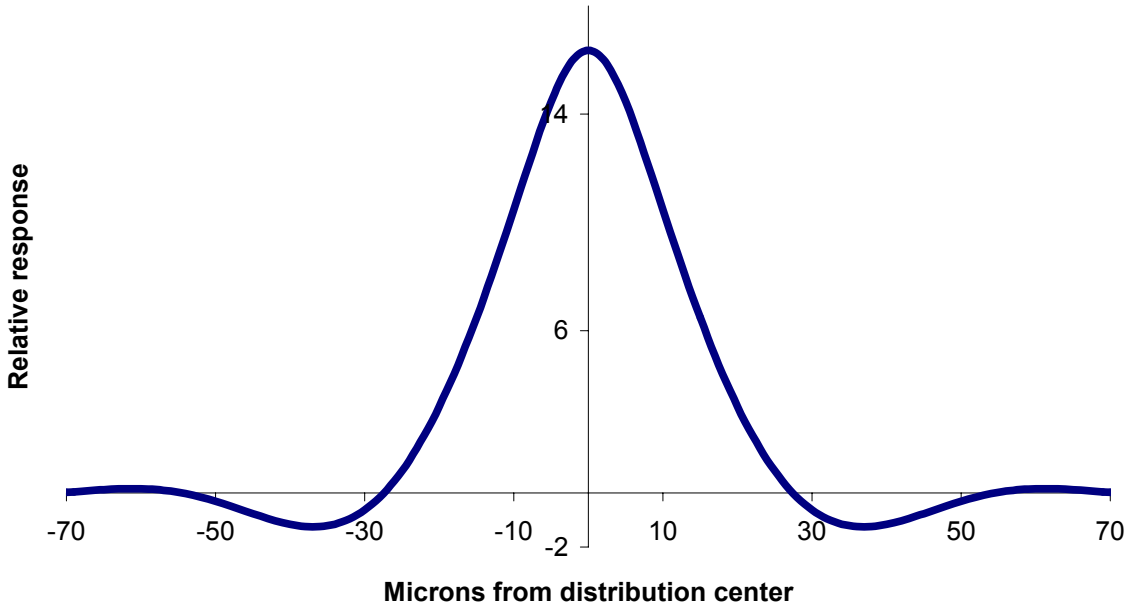

Figure 9 Resolution and single photon data for the 4Q05.

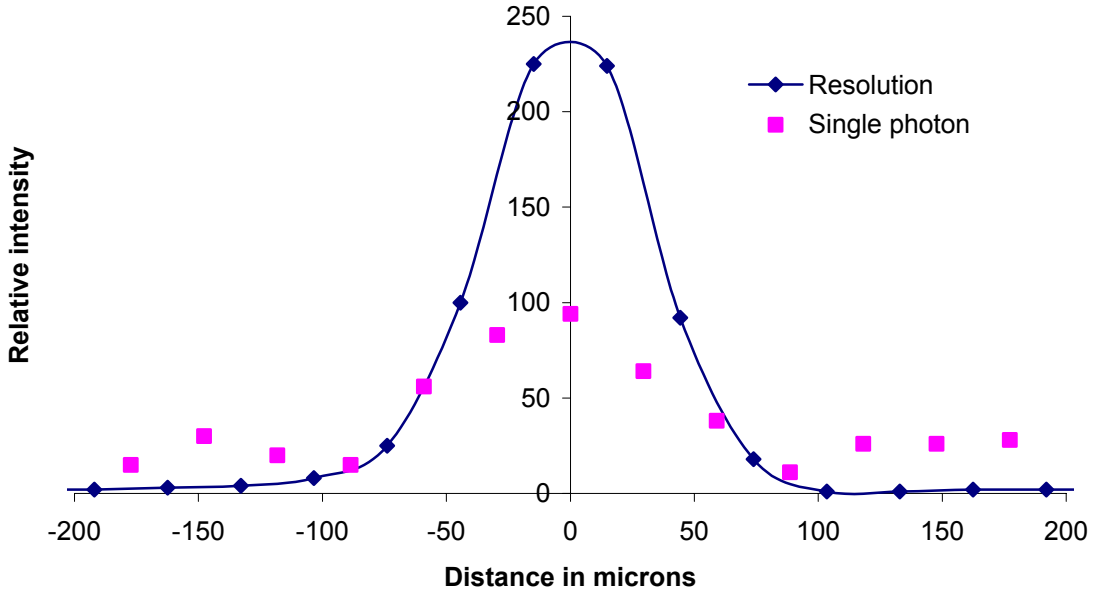

Figure 10. Comparison of single photon distribution and resolution measurement for the 4Q05

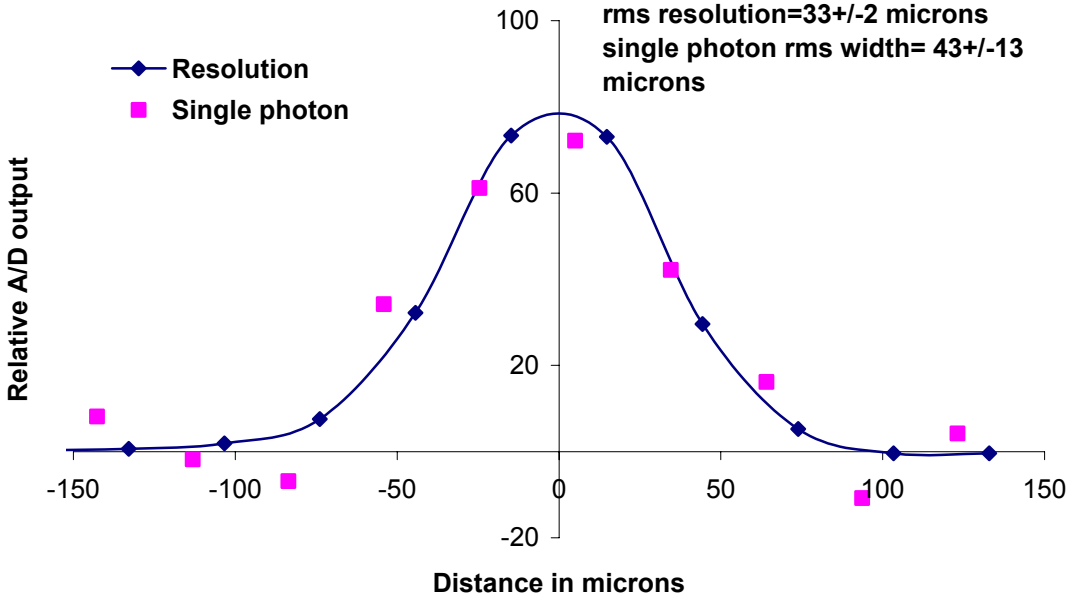

Figure 11. Background Corrected Measured Delta Function Response and One Photon Response for the ISG-250.

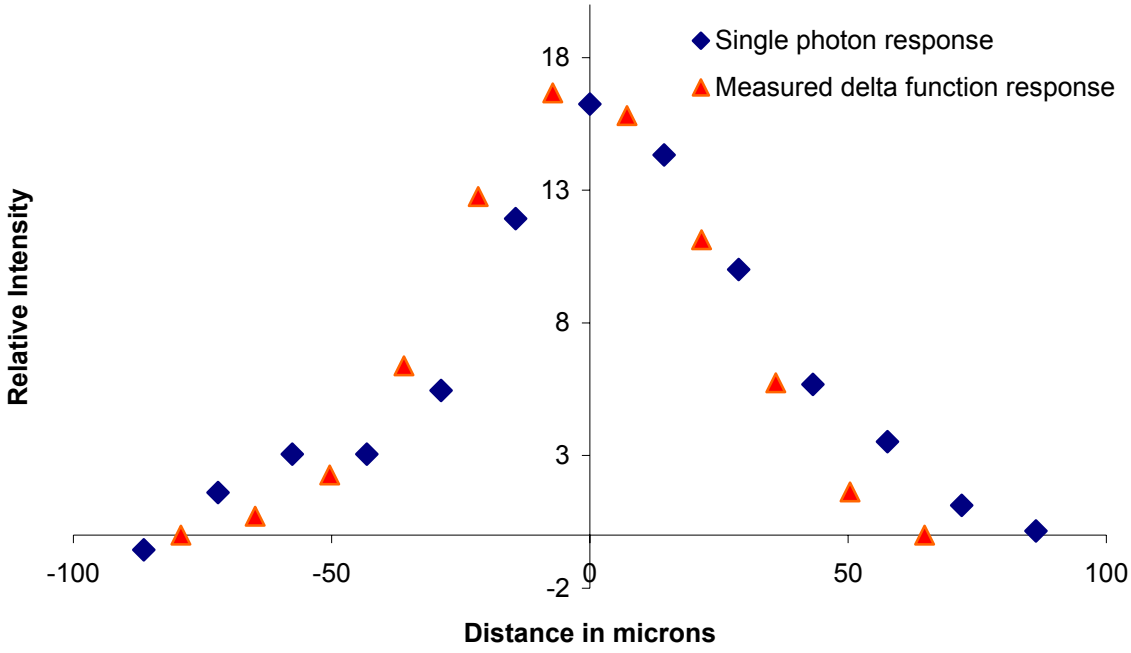

Figure 12. Aberration Parameters

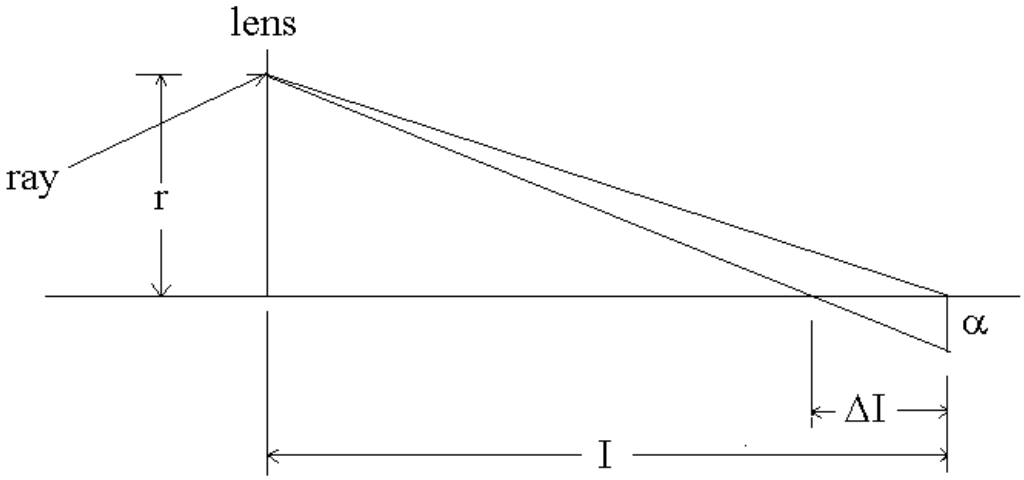

Figure 13. Calculation of average aberration

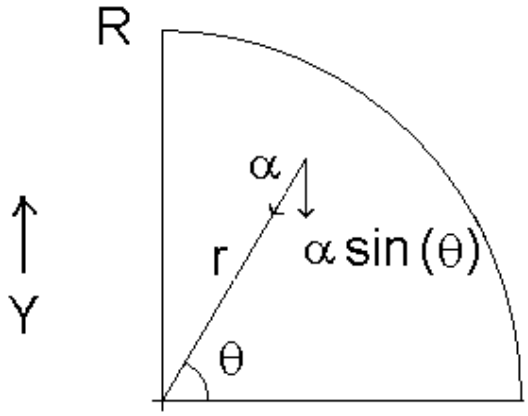

Figure 14. LSO Spectrum

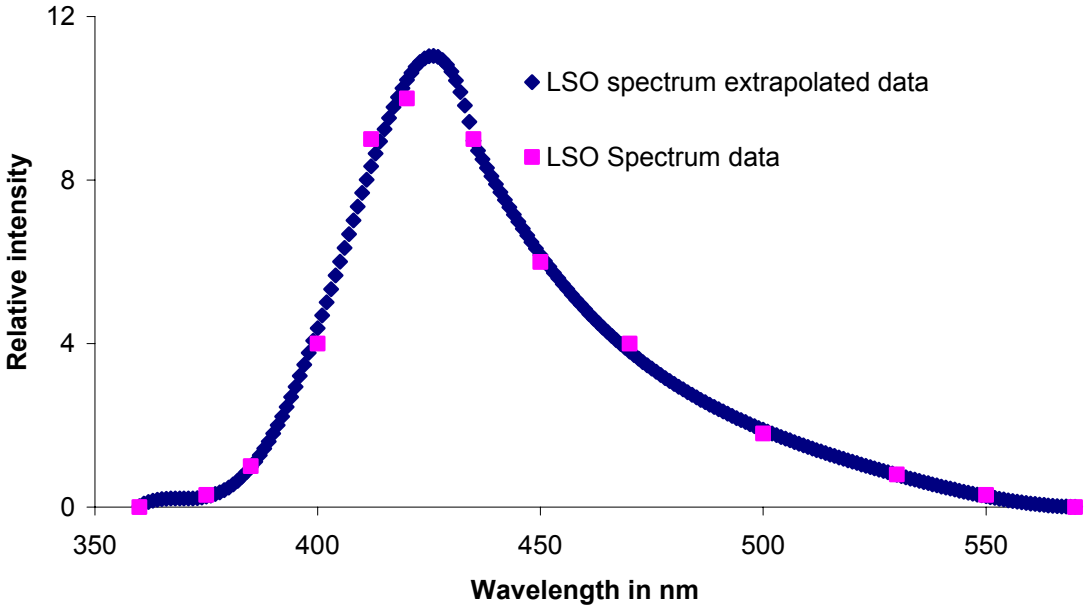

Figure 15. Index of refraction for fused Silica

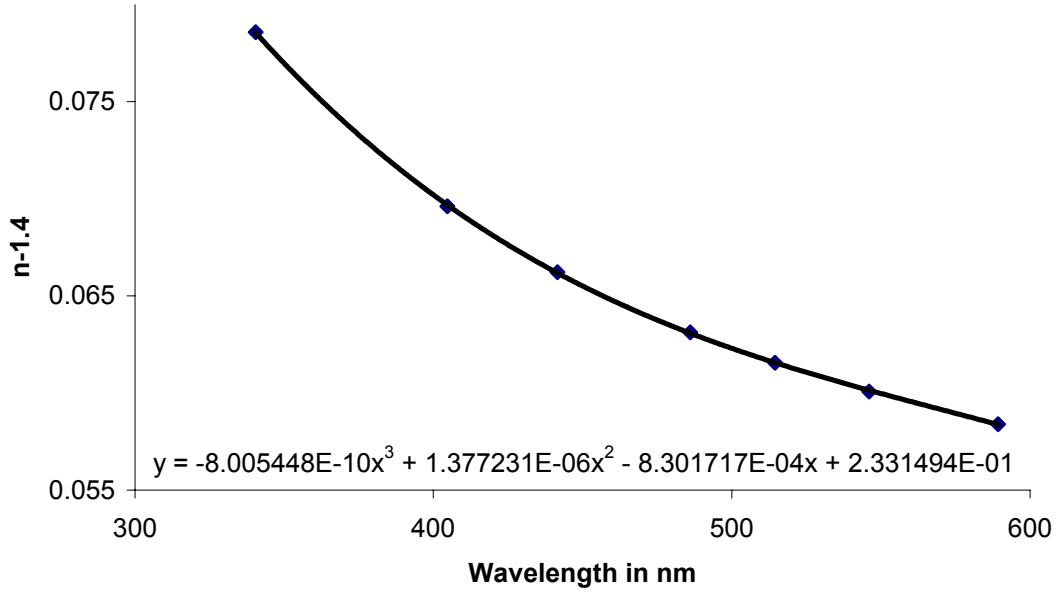

Figure 16. Spherical aberratin calculation

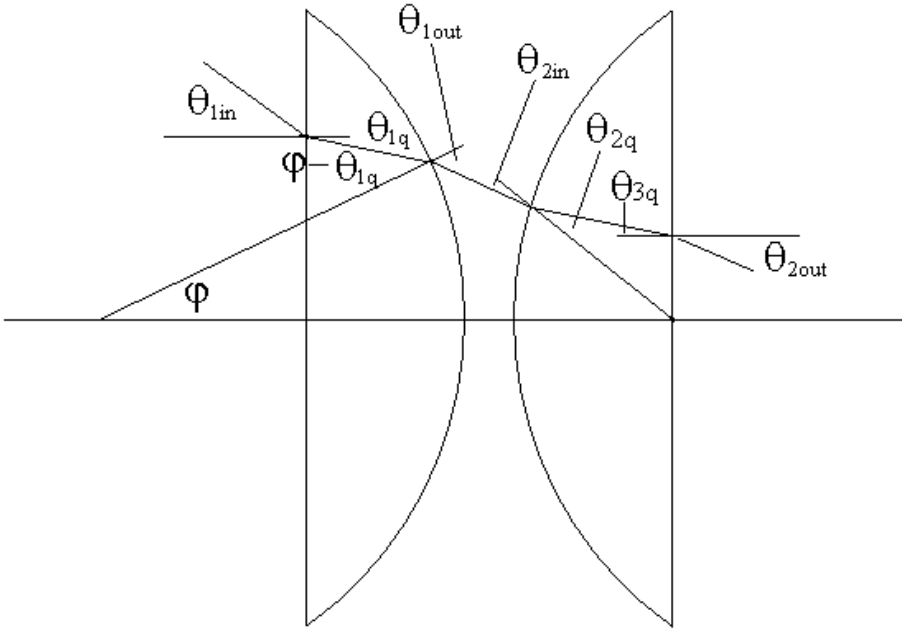

Figure 17. Fused silica achromatic system

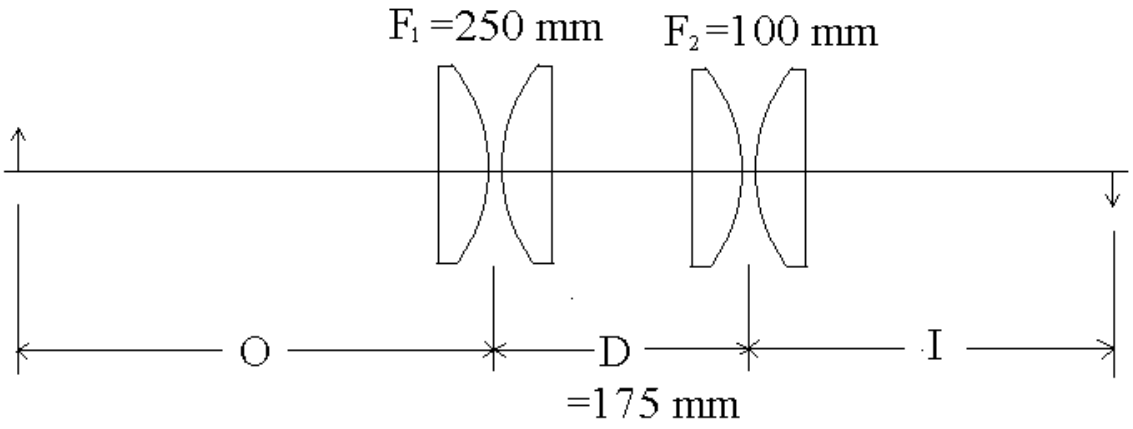

Figure 18. Concept design for viewscreen based beam imaging system

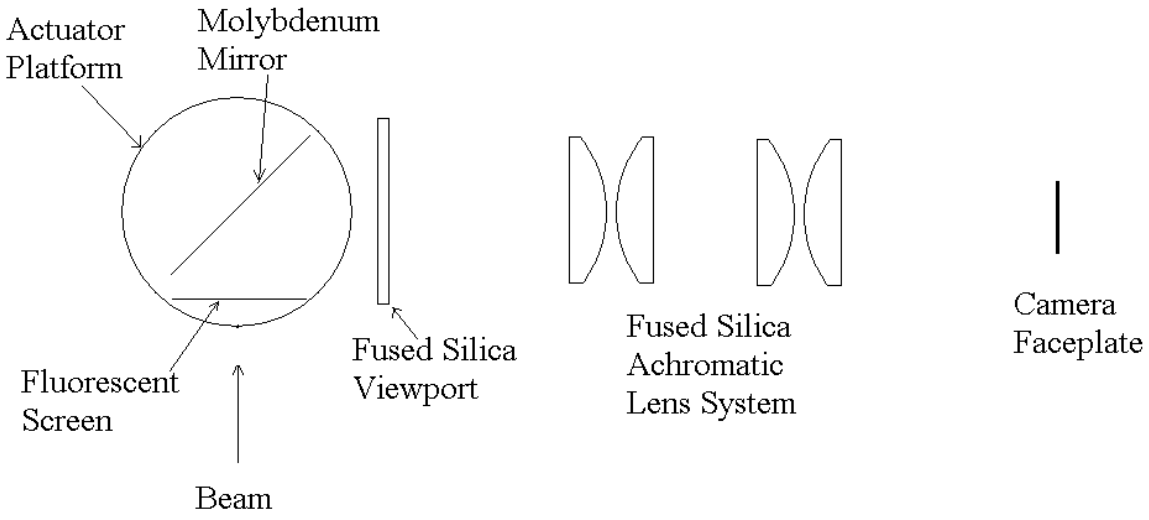

Figure 19. Energy deposition rate by protons in Tungsten.